Per Anton Øverseth Olsen

Analysis of Tripods for Walking Purposes

Masteroppgave i Teknisk Kybernetikk
Veileder: Anton Shiriaev
Januar 2019

Masteroppgave

NTNU
Norges teknisk-naturvitenskapelige universitet
Fakultet for informasjonsteknologi og elektroteknikk
Institutt for teknisk kybernetikk

NTNU
Kunnskap for en bedre verden

Per Anton Øverseth Olsen

Analysis of Tripods for Walking Purposes

Masteroppgave i Teknisk Kybernetikk
Veileder: Anton Shiriaev
Januar 2019

Norges teknisk-naturvitenskapelige universitet
Fakultet for informasjonsteknologi og elektroteknikk
Institutt for teknisk kybernetikk

Problem Formulation

The main objectives are:

- Modeling of the three-legged locomotive robot.
- Analysis of how mass distribution influences the model among other properties.
- Analyze possible motions relevant for walking purposes for the robot.
- Reveal if particular configurations lead to specific strategies, or if specific strategies should be avoided for particular configurations.

Preface

This report describes the analysis of models and motions for a ten-link locomotive robot. This task was chosen as a master thesis in robotics at NTNU as part of the study program Engineering Cybernetics, during the autumn 2018 and winter 2019. The author chose this task because of a general interest in locomotive, legged robots. Also, the author wanted to study a type of robot which does not appear often in the literature and practical applications.

Trondheim, 2019-17-06

Per Anton Øverseth Olsen

Acknowledgement

The author wants to thank Prof. Anton Shiriaev, for providing relevant literature, advise regarding the structure of the report, and letting me contribute to this field of research, and Maksim Surov, for helping with the last finish of the report as well as advise regarding the mathematical problem solving.

Abstract

The environment surrounding humans consists of areas where wheels are not optimal for locomotion. Hence, legged robotics has potential to expand the availability of machines in environmental challenging areas. Some architectures, as bipeds, quadrupeds and hexapods, have in general been more popular. Analysis of the dynamics of a three-legged locomotive robot, called *the tripod*, can reveal benefits and disadvantages compared to the other architectures. Analyzing the dynamical properties of a legged locomotive robot consists of modeling of the dynamics and investigating the possibility and properties of gaits. The robot models were developed using d'Alemberts principle of virtual work and Euler-Lagrange method of generalized forces together with impact models based on Newton's Impact law. The dynamic models, roughly categorized as *the simple model* with platform mass considerably larger than leg masses, *the semi-simple model*, with platform mass and masses in the knee joints, and *the full complexity model* with masses and inertias for each link were calculated and simulated using MATLAB. The specific joint torques needed for the platform to follow different trajectories, while supported by all three legs, are presented and simulated for some cases. This is an over actuated system with geometrical dependencies. Motions describing lifting of one leg is presented, in addition to the dynamics of the following pendulum-like behaviour of the two-leg stance. A motion generator was developed for the semi-simplified tripod, under some assumptions, which proved to be undesirable. Some strategies for repositioning of the leg and especially lifting the leg proved to be more robust for the simplified model.

0.1 Sammendrag

Miljøet mennesker omgir seg i består av områder som ikke er optimale for forflytning med hjul. Av denne grunnen, har roboter med bein potensiale til å ekspandere fremkommeligheter i utfordrende miljøer. Noen arkitekturer, som tobeinte, firebeinte og seksbeinte roboter har generelt sett vært mer populære. Analyse af dynamikken til en trebeint forflytningsrobot , kalt *tripod*, kan avdekke fordeler og ulemper sammenlignet med andre arkitekturer. Analyse av de dynamiske egenskapene til roboter med bein består av modellering av dynamikken, undersøkelse av potensielle gangarter og deres egenskaper. Robotmodellene ble utviklet ved å bruke d'Alemberts prinsipp omhandlende virtuelt arbeid og Euler-Lagranges metode med generaliserte krefter, sammen med impulsmodeller basert på Newtons impulslov. De dynamiske modellene, grovt karakterisert som simplifisert modell med neglisjerbare masser til beina, semi-simplifisert modell, med platform-masse og masser i kne, og den helkompliserte modellen der alle masser om treghetsmomenter er medberegnet, ble utledet og simulert ved hjelp av MATLAB. De spesifikke leddmomentene nødvendige for at platformen skal følge forskjellige baner, i tilfellet der platformen er holdt oppe av alle tre beina, er pressentert og simulert for enkelte tilfeller. Dette er et overaktuert system med geometriske betingelser. Bevegelser som beskriver løfting av et bein er presentert i tillegg til dynamikken til den medførte pendellignende oppførselen ved tobeinstillingen. En bevegelsesgenerator ble utviklet for den semi-simplifiserte modellen avhengig av noen antagelser, som viste seg å være uønsket. Noen strategier for reposisjonering av beinet og spesifikt løfting av beinet viste seg å være mer robuste for den simplifiserte modellen.

Contents

Problem Formulation i
Preface ii
Acknowledgement iii
Abstract iv
0.1 Sammendrag v

1 Introduction **1**
1.1 Relevance and history of legged robotics 1
1.2 Three-legged walkers 4
1.2.1 Contributions and structure 5

2 Background **11**
2.1 About the tripod 11
2.2 Three-DOF legs 12
2.3 Generalized coordinates 13
2.4 Dynamic equations 14
2.4.1 D'Alembert's principle of virtual work 14
2.4.2 Euler-Lagrange equations 15
2.5 Impact models 17
2.5.1 Inelastic and elastic impacts 18
2.5.2 Impact for a constrained Euler-Lagrange system 19
2.5.3 Development of impact models based on experiments 19
2.6 Simulation and validation of models 21

2.6.1 Numeric calculation of solutions to multi-dimensional ODE . 21
2.7 Virtual holonomic constraints 22
2.8 Motion planning for underactuated system 23

3 Methodology **25**
3.1 Modeling 25
3.1.1 Different coordinate system configurations 25
3.1.2 Simple model 28
3.1.3 The Euler-Lagrange models 36
3.1.4 Simplified and semi-simplified model of tripod during two-leg stance 39
3.1.5 Impact models 45
3.1.6 Impact models on Lagrange-form 46
3.2 Design of motions for the tripod 47
3.2.1 Repositioning of a single leg 47
3.2.2 Analysis of configuration space and trajectories 48
3.2.3 Movement of platform during three-leg stance using simplified model 51
3.2.4 Two-leg stance for tripod model with leg masses << platform mass 56
3.2.5 Motion planning for semi-simple model 60
3.2.6 Movement of platform during three-leg stance with non-zero leg masses 67
3.3 MATLAB code 68
3.3.1 Setting up simulation framework 68
3.4 The physical tripod 70
3.4.1 The leg construction and design 70

4 Results **75**
4.1 Three-leg-stance 75
4.2 Two-leg-stance 80

4.3 Model in Gazebo 86

5 Discussion **87**

5.1 General observations 87

5.2 Development of necessary tools 87

5.3 Representation of the coordinates 89

5.4 Usefulness of a simplified model 90

5.5 Three-leg motion 90

5.6 Two-leg motion 91

6 Conclusion **93**

6.1 Future work 94

A Acronyms

B Equations

B.1 Theorems and lemmas . . . . . .

B.2 calculated values and relations . . . . . .

List of Figures

1.1 A platform with four legs standing on a surface. The sections on the floor depict the tilting axes if one leg is longer or shorter 4

1.2 Overview of the ten-link tripod analyzed in this report. 6

1.3 A graph describing the various models and how they developed. . . . 9

2.1 Three-DOF leg referred to as *insect-leg*. 12

3.1 Coordinate systems: the initial frame, platform frame. 26

3.2 Location of the feet coordinate system frames: foot A, foot B, and foot C. 27

3.3 External forces acting on the tripod 29

3.4 Transformation vector from hip-platform connection to feet 33

3.5 Configuration polygon with CoP located on the inside 35

3.6 Leg when platform mass >> leg mass 37

3.7 Leg when platform mass >> leg mass 40

3.8 The semi-simple model includes masses on knees based on 3.2 42

3.9 The semi-simple model includes masses on knees based on 3.2 and 3.1 43

3.10 Overview of four different ways of repositioning the swing leg. The gray lines indicated the next position. 48

3.11 The projection of center of mass in to different positions at two different times 52

3.12 Phase portrait of the semi-simple dynamics with fixated values associated with equation 3.101. The point $(\phi_0, \dot{\phi}_0) = (0, 0)$ can be recognized as an unstable equilibrium [14]. 61
3.13 Phase portrait of the semi-simple dynamics with fixated values as in 3.12, with the motion generator in equation 3.106. 63
3.14 The desired motion for the motion when starting two-legged stance with initial position of the CoP outside the CP 64
3.15 Picture of an almost completely assembled robotic leg, attached to the platform bracket. 72
3.16 Picture of a motor driver designed and produced as part of the overall project. 73

4.1 Plot of distance between the back foot and the center of pressure for the simplified tripod, based on the parametrization in equation 3.46. The other parameters are: $M = 1$, constant length $d_2, d_3 = 0.4$, $\theta_{2_0} = \pi/6$,$\theta_{3_0} = \pi/3$, height of the configuration polygon $h_c = 0.5$, #Steps = 10000 76
4.2 Plot of angles associated, and with same parameters as in 4.1 76
4.3 Plot of the torques for the back leg associated and with the same parameters as figure 4.1 77
4.4 Plot of distance between the back foot and the center of pressure for the simplified tripod, based on the parametrization in equation 3.46. The other parameters are: $M = 1$, constant length $d_2, d_3 = 0.4$, $\theta_{2_0} = \pi/3$,$\theta_{3_0} = \pi/3$, height of the configuration polygon $h_c = 1$, #Steps = 10000 77
4.5 Plot of angles associated, and with same parameters as in 4.4 78
4.6 Plot of the torques for the back leg associated and with the same parameters as figure 4.4 78
4.7 Plot of the torques for the back leg associated and with the same parameters as figure 4.4, but with an additional constant force of 1 newton in the negative x axis 79

4.8 Plot of the torques for the back leg associated and with the same parameters as figure 4.4, except for the mass, which is 0.5 kg 79
4.9 Plot of angle ϕ_1 as the perpendicular force for varies in magnitude, with duration of half a second. The other parameters are: $m = 1$, constant length $d = 0.9$ meters which is relevant for the physical tripod. #Steps = 10000 80
4.10 Phase portrait of the simple dynamics with normalized arrows. The parameters are the same as in plot 4.9 81
4.11 Phase portrait of the semi-simple dynamics with normalized arrows. The parameters are the same as in plot 4.9, except for the knee mass $m = 0.5$, with the motion generator shown in Appendix B.2 82
4.12 Angle of the generalized coordinate associated with the position of center of mass with same parameters as 4.11 83
4.13 Motion of the actuated coordinate with the initial conditions indicated and motion generator shown in equation B.2 in Appendix . . . 83
4.14 Phase portrait of the semi-simple dynamics with normalized arrows. The parameters are the same as in plot, with the motion generator shown in Appendix B.2. Here the initial velocity is positive in $t = 0$ 84
4.15 Angle of the generalized coordinate associated with the position of center of mass with same parameters as 4.11 85
4.16 Motion of the active coordinate with the initial conditions indicated and motion generator shown in equation B.2 in Appendix 85
4.17 Picture from simulation of the passive dynamics simulated by gazebo's internal physics motor. $t = t_0$ 86
4.18 Picture from simulation of the passive dynamics simulated by gazebo's internal physics motor. $t = t_1$ 86

List of Tables

1.1 Description of the assumptions in the tree 1.3 8

2.1 Description of the variables and parameters in section 2.5 18

3.1 Denavit-Hartenberg table of the complete robot from platform to feet for leg i, from [29] 27

3.2 Denavit-Hartenberg table of the complete robot from stance leg to feet for leg i 28

3.3 Description of the variables and parameters in section 3.1.2, and their associated spaces. See figure 3.4 for details on joint parameters and and variables. Part 1 30

3.4 Description of the variables and parameters in section 3.1.2, and their associated spaces. See figure 3.4 for details on joint parameters and and variables. Part 2 31

3.5 Description of the symbols in the matrix 3.10 and the gravity vector 3.13 38

3.6 Description of the symbols in equations 3.16 to 3.18 41

3.7 Description of the symbols in equations 3.19 to 3.23 44

3.8 Overview of the different outcomes of impact for the tripod. $\oplus$ indicates exclusive or. 46

3.9 Overview of the different MATLAB functions and scripts used in this thesis. 69

3.10 A description of measured values for the electric motors used on the early prototype physical tripod. Working torque T_1, stall torque T_2, voltage and current were measured and described in [30]. 74

Chapter 1

Introduction

1.1 Relevance and history of legged robotics

In contrast to the continuous contact with the surface resulting from wheels and belts, legged locomotion uses discrete points on the surface, sequentially, to move the rest of the body continuously. This has some immediate advantages when it comes to different challenging surfaces. [36] claims that around fifty percent of the earth's surface is inaccessible to traditional wheeled vehicles. Building roads fit for wheel or belt-transportation can damage vulnerable environments and in many cases becomes impractically costly. The importance of development of vehicles able to travel through these areas, without introducing lasting damage, is increasing as we investigate remote locations on Earth and in space. The surfaces challenging for wheeled locomotion exists in natural environments, catastrophe-areas and many areas designed for human walking [36].

Because of technical difficulties regarding legged robotics, successful attempts of dynamic walking using four or less legs have been rare before the millennium. Still, most of the legged robots currently in use are connected to research rather than problem solving in industry. Some examples of recent successful robots designed for walking dynamically in a variety of environments are Atlas and Spot, devel-

oped by Boston Dynamics and ASIMO developed by Honda[4]. The main reasons for the rapid development of walking robots are the computer technology, strong and precise electric motors, and development of relevant mathematics and motion studies [36]. Researchers began investigating the field of legged robotics in the 1950's in a systematic way, and ten years later prototypes began showing up. The 1960's legged robots used conservative control strategies demanding powerful actuators with high energy consumption, and were hard to steer. The problems at that time were mostly due to the limited understanding on leg coordination control and walking gaits, difficulties developing practical machine legs, and limited computing capability. Today the main problem is not computing power, but rather construction of practical machine legs[1] and integration of different techniques to achieve robustness in different environments.[2] claims that the third stage of cybernetics and robotics development, characterized by algebraic progress, is still going on today[2]. Even if legged locomotion has some advantages when it comes to challenging terrain, the disadvantages when it comes to speed, control complexity and mechanical complexity, compared to different wheel and belt-driven vehicles, makes walking machines rare in practice. Fast motion of the body requires faster moving legs and/or long legs. Moving parts usually change direction one or more times during every step. This causes wear and tear on bearings [3][3]. In addition impulse forces damage mechanical components such as bearings and fragile parts. [4] mentions this was a problem for the testing of the robot called Rabbit, a bipedal locomotive robot. In [32], a failure matrix summarizes possible bearing failures due to shock loads and vibrations. These involve fatigue, wear damage, plastic deformation problems, fracturing and cracking. There are methods to reduce wear caused by switching directions as well as spring damping systems that can avoid destructive shock forces, however this increases the system complexity and cost.

Concerning three-legged robotics, the previous research is limited. Despite the fact

[1] Especially actuators that are strong, accurate, light, and fast.

[2] At least between 1970 to 2000

[3] Walking robots which uses wheels with legs are considered to be wheeled robots in this report.

that three legs provide minimal static stability, only very specialized problems are solved using three legs. When standing still on an uneven surface with more than three legs, the benefit of a larger *configuration polygon*[4] is prominent regarding prevention of falling. However, in terms of precision, a small deviation in the length of one leg, or equivalently an unexpected elevated area of the surface, leads to a tilting axis, if the other legs does not equalize this difference. For a construction with an even[5] number of evenly distributed legs, the center of pressure usually comes near the tilting axis, which is an unstable equilibrium. These axes are depicted in figure 1.1. Small disturbances can hence cause tilting. Minimal design together with the need for high precision is the main reason the *NanoWalkers* in [22] has three legs. The NanoWalker's legs however, differs from usual robotic legs, as they are piezoceramic actuators, and the gaits depend on friction constants and other material properties. Robots used for demining missions are in some cases quadropeds, but the risk of unintentional explosion vitalizes development of gaits where one or two legs are missing. In [17], this problem is addressed, and a solution is presented. The demining robots use robotic manipulators, more commonly used in general robotics, and more relevant for this report. The *kick-and-swing gait* is however, based on a number of assumptions which limit the controllability and makes the results less relevant for the general tripod. More specifically, these assumptions are; massless legs, non-slipping support legs, and the collision of leg with ground is inelastic. Three-legged robots developed for purely scientific reasons, as the simple spring-servo actuated robots in [23], comes in different shapes. The purpose of the latter research is to investigate the reason for lack of animals on three legs in nature. The simplicity of the robot limits the possibility of many conceptually different gaits, and these gaits are specifically generated by using periodic oscillations for the muscle-like actuators. The lack of specific research on the general tripod with insect-like[6] legs makes the literature on bipeds relevant.

[4] CP, (the area spanned between the feet at ground)

[5] An odd number of legs does not lead to tilting axes directly in the middle.

[6] Legs with a two-DOF hip joint and a knee, often seen i hexapod toys and similar robots

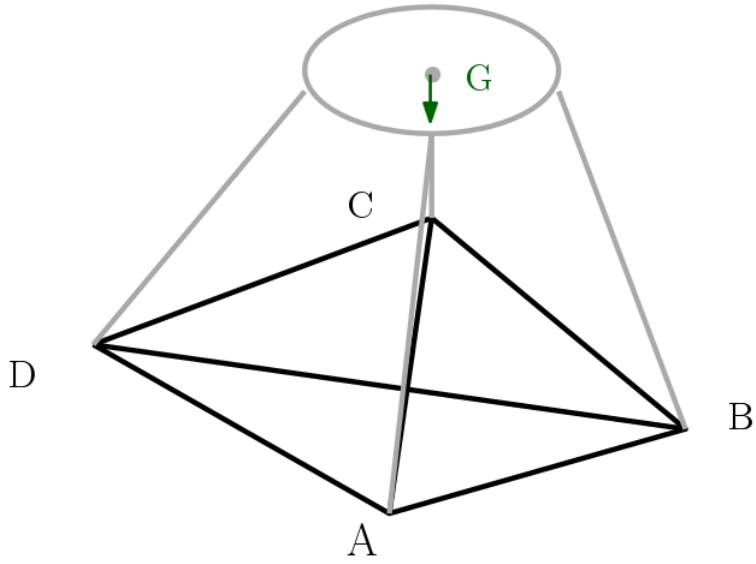

Figure 1.1: A platform with four legs standing on a surface. The sections on the floor depict the tilting axes if one leg is longer or shorter

1.2 Three-legged walkers

The lack of DOF and/or the lack of link complexity of models make the prior research on tripod limited to certain gait families. Statements regarding why the mathematical models are simplified and comparisons of the models are lacking. Often the main goal is not the mathematical model, but rather the methodology, such as in [23]. In many cases simplifications are either necessary to gain understandable information about the system, or a simplified model can be sufficient for the specific task, not demanding further analysis. As tripedals are so rare in the robotics literature, a general analysis of the subject is desirable.

Analysis of gaits for a N-DOF three-legged walker, considering realistic impact models and full dynamics of legs, might introduce other gait patterns that are more energy effective, faster or more robust than previous gaits for tripedals. Analysis of gaits and models which uncover weaknesses in terms of these mentioned factors adds equally important knowledge to the subject. The level of complexity of the different models depends on many factors. From the previous project [29], a

high level of complexity is expected for the least simplified models. Restricting the model will reformulate the problem in various ways. The robot kinematic graph and parameters of the tripod investigated in this report are tightly embedded in a larger project consisting of building the physical tripod, its electronic components and payload. As the physical design procedure has pursued for almost a year, an early version prototype is under construction with complete electronic modules and some mechanical parts. The parameters of this prototype is used as a basis for this study. For the prototype, lots of factors such as joint friction, slack in gears, elasticity of links and in gears, finite resolution of sensors, and friction forces between surface and feet can introduce additional complications. Some of these factors will be addressed in this report. The main goal is however, development of a mathematical basis. Analysis of a general tripod with associated tripod gaits, or motions relevant for gaits, is needed, as well as comparisons between different models.

The tripod robot investigated in this report is a ten-link, triradially symmetric walker with passive feet, where each leg has three DOF and rotational actuators connected to the platform. In connection to the surface, when standing still or moving, the number of degrees of freedom is dependent on which friction assumptions are made, and number of legs in contact with ground. A figure depicting the tripod can be viewed in figure 1.2[7].

1.2.1 Contributions and structure

In this report, several models are analyzed. Firstly different approaches regarding coordinate frames are presented. Together with different assumptions and geometrical simplifications, these give rise to a number of models with different number of DOFs. The full model with masses and inertias of every link is developed, but

[7]Note that the other representations of the tripod shows a circular platform. This is closer to the physical tripod

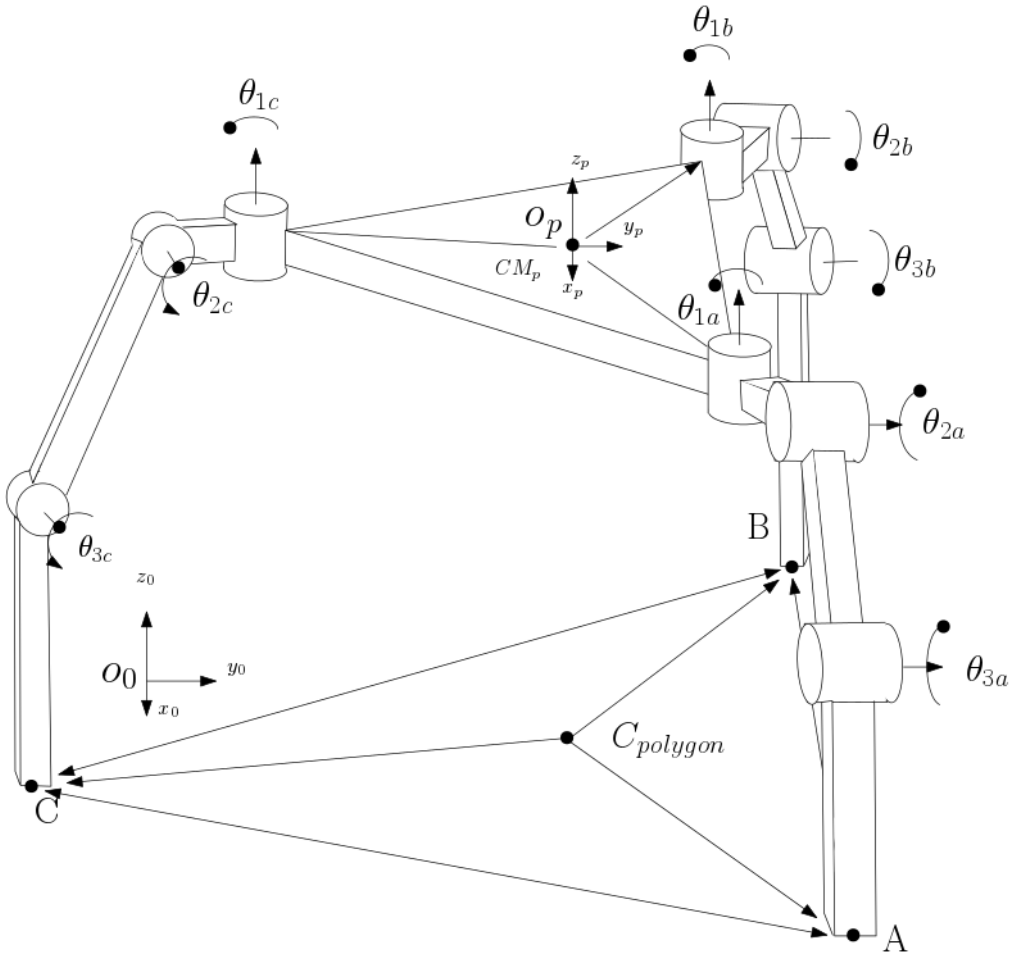

Figure 1.2: Overview of the ten-link tripod analyzed in this report.

simplifications are necessary in order to benefit from the information. Different models and considerations regarding the three-leg stances are analyzed briefly for various models. Torques as a function of time is derived from these equations. The dynamics of the three-leg stance leads to a strategy for lifting a leg, leading to the two-leg stance. A simple model similar to the ones described in [17] and [13], is analyzed, focusing on the two-leg stance, where the support-leg joints are fixated. Dependent on where the desired next position of the swing leg foot is, one strategy was found not to be robust when leg masses and inertias are considered small in contrast to the platform mass and inertia. For the slightly more complex model, with added masses to the knee-joints, a similar tendency was detected, suggesting similar gaits for this model.

This report starts with a brief representation of the key points regarding background theory. The main part, describing the methodology, shows how the models were developed, associated motions and assumptions in addition to different limitations. Here, the first part will focus on the different models, and the second part will focus on their associated motions. As these are tightly connected, there are some intersection. These mentioned chapters lead to some results presented, before discussion, conclusion and future work. Lastly, acronyms and some equations are presented in the appendix.

There are many models with associated findings. The connection and main development of these models and motions are depicted as a tree[8] in figure 1.3. The nodes with blue color is also calculated in MATLAB.

[8] It is actually not a tree, but a simple graph

Designator	**Assumption**
A1	Leg-masses are eliminated
A2	The platform is a rigid object, not rotated in pitch and yaw, and the back leg is on the symmetry axis
A3	The joint variables of the stance legs are fixated/constant
A4	There are no sudden changes in velocities at the contact points
A5	The robot is considered a rigid solid
A6	The platform orientation aligns with the initial frame
A7	CP is an equilateral triangle
A8	$sin(\alpha) \approx \alpha$
A9	The displacement of CM is sufficiently small

Table 1.1: Description of the assumptions in the tree 1.3

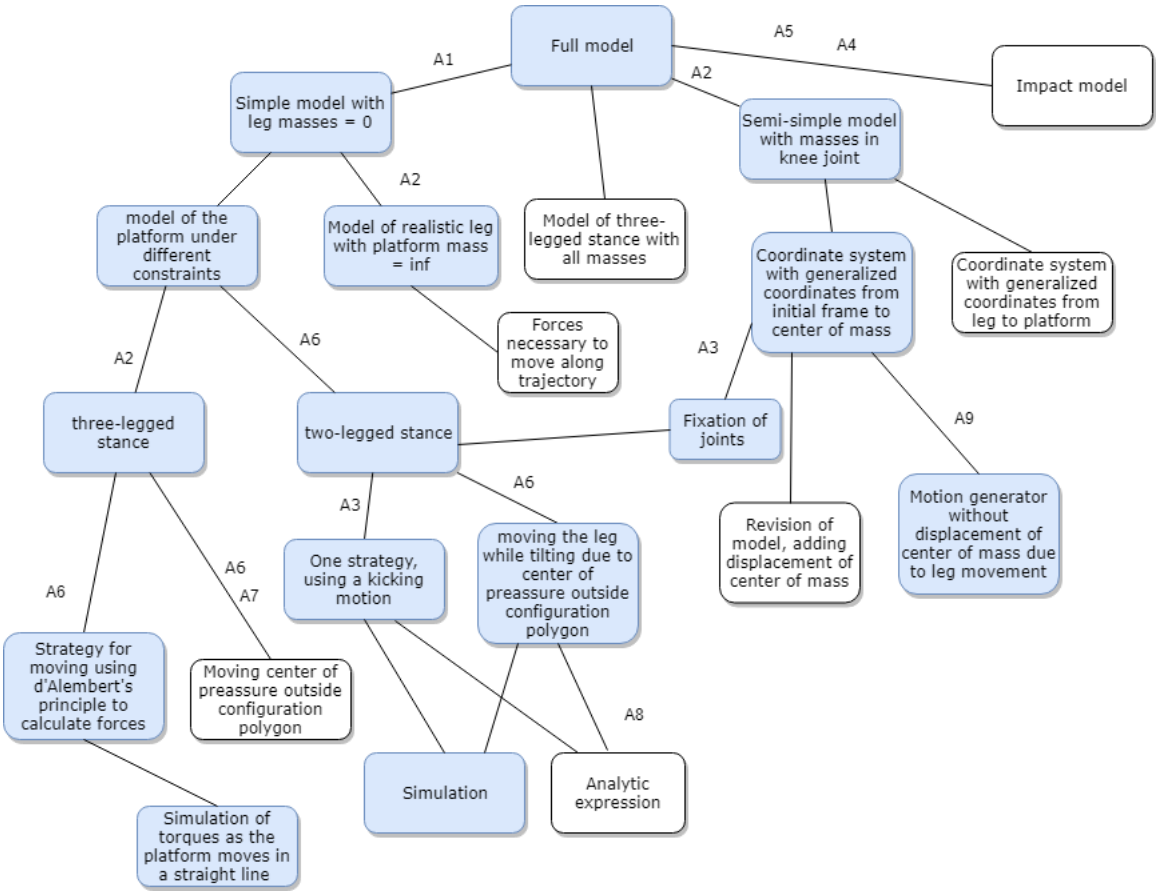

Figure 1.3: A graph describing the various models and how they developed.

Chapter 2

Background

This chapter gives a brief overview of the theoretical concepts which lies behind the development of different models and heuristics.

2.1 About the tripod

The geometric properties of the tripod are not fixated. The robot, called *the tripod*, was previously investigated during the introductory project [29], and has a physical realization which currently[1] is under construction. This physical robot will be called *the physical tripod* in this report. The mechanical, electrical, and other specifications of the physical tripod can be found in [30]. Even if the analysis in this thesis is not restricted to the geometrical and physical properties of the physical tripod, some of the simulations and calculations will be using these values. For the total tripod project, which spans a wider purpose than this report alone, a minimalistic, but not too restricting, design was desirable, because of the projects economy, available computational power and the model complexity. Hence, different N-DOF legs with rotational actuators were considered. Linear actuation was not desirable as the actuators are in general more expensive, complex to make, or

[1] in 2019

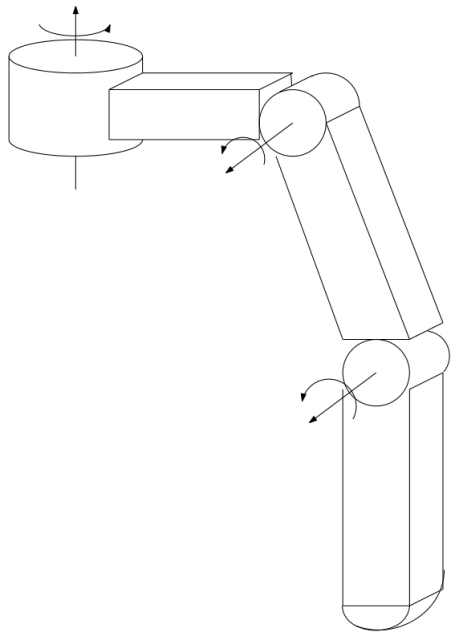

Figure 2.1: Three-DOF leg referred to as *insect-leg*.

require many extra components compared to the simple servo motors. A visualization of the tripod can be viewed in figure 1.2. This project will be mentioned later in this report.

2.2 Three-DOF legs

There are many different ways of constructing three-DOF legs. The insect-like design, as in figure 2.1, was chosen as it is one of the revolute joint realizations, fit for placing the motors with gear boxes such that the inertia is minimized. The mass of the motor and gear-box is the main contribution to the total mass of each link, and the placement of these components are crucial considering the leg inertias. Note that an additional rotational joint at the hip[2] of the robot expands the configuration space of the tripod.

[2]The two joints (in this example, three) attached to the platform is called the *hip* in this thesis.

2.3 Generalized coordinates

There are several ways of describing the positions and velocities of a multi-link robot. Important variables are positions and velocities of the centers of mass for each link, and the rotational equivalents. These variables are needed in order to derive the equations of motion for the system. Coordinates which describes the joint variables are also needed in order to describe the configuration of the robot. As both orientation and position of each link in three dimensional euclidean space, is important, some strategies are better than others. Excessive coordinates (x_p, y_p, z_p) can describe the centers of mass in the coordinate system p, and similar vectors can describe the joint positions, and the feet positions. However, this quickly becomes overly complex. The notion of coordinate frames attached to each separate link is therefore a more suitable strategy. This can be achieved by using *homogeneous transformations*. These are a subset of affine transformations [20] in three dimensional space described with four dimensional vectors and matrices in $\mathbb{R}^{4x4}$. The homogeneous transformations form a group called *Special Euclidean Group* [10]. These are specified in greater detail in [37] and in the prior report [29].

The same transformation between frames can be expressed in more than one way with use of the general rotations. Most robotic joints, including the joints for the tripod, consist of pistons moving linearly or simple revolute hinge joints. This makes the description of the positions and orientations of links, as well as the inverse kinematics, unnecessary complex in the case of the description by general rotations. A solution to this is the Denhavit-Hartenberg convention. This convention is based on two rotations, and two translations,

$$A_i = R_{z,\theta_i} T_{z,d_i} T_{x,a_i} R_{x,\alpha_i}. \tag{2.1}$$

Even if the D-H convention does introduce generalized coordinates, the description of position and orientation of a 6-DOF solid still requires six generalized coordinates using D-H. In these cases, the general rotation and translation might be more intuitive.

Where D-H convention or general rotations does not represent the different link positions of a multi-link robot in a intuitive way, excessive coordinates can also considered. However 3-D space introduces three coordinates for each link, and rotations often becomes challenging to represent.

2.4 Dynamic equations

This sections will briefly describe which methods are used when deriving dynamic equations for robot systems. A key concept for a system without dissipative forces and distributed parameters is the law of conservation of mechanical energy. In section 2.3 we saw that generalized coordinates can reduce the number of equations for a system. For example, dynamics of two a link pendulum can be written in excessive coordinates (x_1, y_1) and (x_2, y_2) (Cartesian coordinates of mass centers of the links), or in generalized coordinates θ_1 and θ_2 (angles between links and the vertical plane). For some robotic systems, the usage of generalized coordinates could introduce extra confusion instead of a simplified dynamics. However, the Denavit-Hartenberg convention provides generalized coordinates which in many cases leads to a huge reduction in number of equations.

2.4.1 D'Alembert's principle of virtual work

In dynamics, the concept of virtual work is important. It helps to bind displacements of a mechanical system in 3D space, forces, torques acting on the system, and displacements of the generalized coordinates, and generalized torques [8].
Now, consider an example, a system from N freely moving rigid bodies in 3-D space. The system has $6N$ degrees of freedom[3]. However, if geometrical constrains are present between the rigid bodies (for example, hinges and prismatic joints) then the system will have fewer degrees of freedom ($< 6N$). These geometrical

[3]Note that a rigid body has orientations and positions, meaning 6-DOF if there are no geometrical constraints

constraints are due to forces of constraints or *reaction forces*. If the constraints are ideal, then they must satisfy the *principle of virtual work* (see [8] for more details)

$$\sum_{k=1}^{N} \delta \mathbf{r}_k \cdot \mathbf{F}_k^c = 0 \tag{2.2}$$

, where $\delta \mathbf{r}$ is the vector of virtual displacement and $\mathbf{F}^c$ is the reaction force.
When the generalized coordinates are independent, d'Alembert's principle of virtual work can be expressed as follows,

$$\sum_{k=1}^{N} \frac{\partial \mathbf{r}_k}{\partial q_i} \big(m_k \frac{d^2 \mathbf{r}_k}{dt^2} - \mathbf{F}_k \big) = 0. \tag{2.3}$$

Here, q_i are the generalized coordinates, m_k the mass of the particle, and $\mathbf{F_k}$ is the external force.

2.4.2 Euler-Lagrange equations

In the following part, consider a mechanical system with generalized coordinates $q \in \mathbb{R}^n$, and holonomic constraints $\phi_k(q) = 0$. The equations of motion for such a system can be obtained using the Lagrange equations of the I-st kind (see [29] for more details),

$$\mathcal{L} = K - P, \tag{2.4}$$

$$\frac{d}{dt}\Big[\frac{\partial \mathcal{L}}{\partial \dot{q}_i}\Big] - \frac{\partial \mathcal{L}}{\partial q_i} = \sum_k \lambda_k \frac{\partial \phi_k}{\partial q_i}. \tag{2.5}$$

In equation 2.5, P is total potential energy of the system, K is total kinetic energy of the system, q_i is the i-th generalized coordinate, λ_k is the k-th Lagrangian multiplier, and ϕ_k is the k-th holonomic constraint. This is explained in greater detail in [37].
As 2.5 shows, the method requires one to evaluate the total kinetic and potential energy of the system. The potential energy can be calculated directly from the centers of mass of each link and the gravity vector as given in[4],

$$P_i = m_i g \begin{pmatrix} 0 & 0 & 1 \end{pmatrix} \cdot H_i^0 \cdot \mathbf{l}_i. \tag{2.6}$$

[4]If the multi-link system is affected by other conservative forces like magnetic fields or similar this might be more complicated

This procedure is described in [37]. Here, m_i is the mass of link i, H_i^0 is the homogeneous transformation matrix describing position and orientation of link's frame with respect to the initial frame, and $\mathbf{l}_i$ is the position of center of mass of link i given in the link's frame. The potential energy is a scalar-valued function $P_i \in \mathbb{R}$.

The angular and linear velocities and their *velocity Jacobians* calculated as in [37] and [5], can be summarized in the equations below,[5]

$$v_n^0 = J_n \dot{q}, \tag{2.7}$$

$$\omega_n^0 = J_\omega \dot{q}, \tag{2.8}$$

$$\omega_n^0 = \sum_{i-1}^{n} \rho_i \dot{\mathbf{q}}_i z_{i-1}^0, \tag{2.9}$$

$$v_n^0 = \dot{o}_n^0 = \sum_{i-1}^{n} \frac{\partial o_n^0}{\partial q_i} \dot{\mathbf{q}}_i, \tag{2.10}$$

$$J_\omega = [\rho_1 z_0 \cdots \rho_n z_{n-1}], \tag{2.11}$$

$$J_v = [\frac{\partial o_n^0}{\partial q_0} \cdots \frac{\partial o_n^n}{\partial q_n}], \tag{2.12}$$

$$J = \begin{bmatrix} J_v \\ J_\omega \end{bmatrix}. \tag{2.13}$$

From these equations the kinetic energy, and hence the Lagrangian as in equation 2.5 can be derived as a function of generalized coordinates and generalized velocities,

$$K = \frac{1}{2} \dot{\mathbf{q}}^T \Big[\sum_{i=1}^{n} m_i J_{v_i}^T J_{v_i} + J_{\omega_i}^T R_i I_i R_i^T J_{\omega_i} \Big] \dot{\mathbf{q}}. \tag{2.14}$$

The inertia matrix, I_i, of link i, is a symmetric positive definite matrix. Alignment of the link coordinate system often allows the non-diagonal element to be nullified [18].

For a system with n generalized coordinates, the method of Euler-Lagrange leads to n equations, each associated with the generalized coordinate and the generalized force acting on this coordinate. This system of equations can be quantified in a

[5] These equations are presented in [29]

matrix form,

$$D(q)\ddot{q} + C(q, \dot{q})\dot{q} + g(q) = \tau. \tag{2.15}$$

The matrix D corresponds to the kinetic energy of the system (the expression within the brackets in 2.14). The matrix C can be derived by direct calculation of the *Christoffel symbols*. This equation and details regarding these methods are stated in [37].

2.5 Impact models

When a leg hits the ground, a sudden change of velocities might occur for the different links of the robot. This change of velocities depends on the elasticity and mass of the materials and influences designing strategies regarding gaits. The main considerations is if the impact is completely elastic, completely inelastic or something in between. In addition, the geometric parameters should be taken into account. The easiest friction models are those which depict the extremes. These are for most robots less realistic than na empiric model based on experiments. However, simple impact models are often used in legged robotics [4], [24]. In this section, the easiest impact principles are presented in conjunction with Euler-Lagrange, and lastly alternative empirical approaches for developing realistic impact models are briefly mentioned. Table 2.1 summarizes the symbols used in this section.

Symbol	Meaning	Space
v^+	Velocity of a colliding particle after collision	$\mathbb{R}$
v^-	Velocity of a colliding particle before collision	$\mathbb{R}$
e	Coefficient of restitution	$0 \leq e \leq 1 \in \mathbb{R}$
t^-, t^+	Time right before and right after collision	$\mathbb{R}$
S_j	Generalized applied impacts	$\mathbb{R}$
Q_j	Generalized forces	$\mathbb{R}$
I_i	Unknown Lagrange multipliers	$\mathbb{R}$
r_c	Impacts at the contact points	$\mathbb{R}$
q^-, q^+	Generalized coordinates right before and right after impact	$\mathbb{R}$
x_i	Center of mass for a body i	$\mathbb{R}^3$
f_i	The right hand side of the Euler-Lagrange equation 2.5	$\mathbb{R}$
D_c	Constraint matrix	$\mathbb{R}^{i \times j}$
$M_{i,j}$	The mass matrix	$\mathbb{R}^{i \times j}$

Table 2.1: Description of the variables and parameters in section 2.5

2.5.1 Inelastic and elastic impacts

A collision is called perfectly inelastic if there is no conservation of mechanical energy. In principle, this is due to deformation, but significant deformation due to impact is not a normal case for nondestructive analysis, and is not included in this thesis. For a robot manipulator relevant for this thesis, mechanical energy will mainly be absorbed by dynamic friction forces in the gears for the different joints, and the motors. The perfectly inelastic impact of two objects lead to equivalent velocities after impact. A moving leg will therefore stand still after impact with the floor, according to this model. This can be described as follows,

$$v^+ = -ev^-. \tag{2.16}$$

where the constant e is equal to zero in this case.
The opposite of a perfectly inelastic collision is elastic collision. For this case $e = 1$ (see [21]), and the mechanical energy is fully conserved.

Even if the elastic or perfectly inelastic models are less realistic than an inelastic (not perfectly), a combination of these, where $0 < e < 1$, can be sufficient, when developing motions. An inelastic collision depends on the material and geometry, but can in many cases be modeled by a mass spring damper model.

2.5.2 Impact for a constrained Euler-Lagrange system

For a constrained Euler-Lagrange model such as model 2.5, the impact equations can be derived using the method described in [19], and are shown below,

$$S_j = \lim_{t^- \to t^+} \int_{t^-}^{t^+} Q_j t \, dt, \tag{2.17}$$

$$\lim_{t^- \to t^+} \int_{t^-}^{t^+} I_i \, dt = r_c, \tag{2.18}$$

$$q_i^- = q_i^+ \tag{2.19}$$

where

,

$$Q_j = \frac{\partial x_i}{\partial q_j} f_i. \tag{2.20}$$

Integration of the equations of motion from t^- to t^+ yields the impact equations,

$$\left(\frac{\partial \mathcal{L}}{\partial \dot{q}_i}\right)^+ - \left(\frac{\partial \mathcal{L}}{\partial \dot{q}_i}\right)^- = S_j - r_i \frac{\partial D_c}{\partial q_i}, \tag{2.21}$$

$$\begin{bmatrix} M_{i,j} & D_{c,i} \\ D_{c,j} & 0 \end{bmatrix} \begin{bmatrix} \dot{q}_j^+ \\ r_c \end{bmatrix} = \begin{bmatrix} M_{i,j}\dot{q}_j^- + S_i \\ -eD_{c,l}\dot{q}_l^- \end{bmatrix}. \tag{2.22}$$

2.5.3 Development of impact models based on experiments

In desire for a better model, material constants and geometry should be included in the model. The bouncing of a swing leg when it hits the ground can lead to a faulty positioning of the leg, timing faults, and unreliable friction forces. Hence, simplistic models can be dependent on controlled environments in order to function. Analytic models of robotic arms consisting of lots of different materials and

geometries, with several links interacting through the different joints, can quickly become impractically advanced, such that testing would be preferred for the specific robot. The simplest approach is to develop a single spring damper model based on interpolation of maximum and minimum values of relevant velocities and joint positions, with nonpassive joint velocities equal to zero. There exists clear methods for performing such *two-level factorial design* described in detail in [1]. For N parameters with a high and a low value, at least 2^N experiments are needed. Repeating the experiment gives information about the variance. This approach is expandable and can be effective for models where material constants and latent effects are prominent. To derive a model based on these experiments, different methods can be used such as MLR[6], or more advanced methods such as PCR and PLSR. For sensing forces, positions, and velocities for a robotic system, the output is usually a sequence of values, comparable to functions of time, and preprocessing these signals can be necessary.

Another approach on deriving an impact model based on inputs and outputs of an unknown system is *subspace identification methods* such as described in [31][7]. These methods uses input and output matrices for deriving system equations on the standard form,

$$\begin{aligned} \mathbf{x_{t+1}} &= A\mathbf{x_t} + B\mathbf{u_t}, \\ \mathbf{y_t} &= C\mathbf{x_t} + D\mathbf{u_t}. \end{aligned} \tag{2.23}$$

This system can be analyzed using classical control theory such that dampening constants and elasticity factors can be found, or it can be used directly [2].

[6] (Multiple Linear Regression), (Principle Component Regression), (Partial Least Squares Regression)

[7] Different nonlinear variants also exist.

2.6 Simulation and validation of models

2.6.1 Numeric calculation of solutions to multi-dimensional ODE

There are different ways of computing the solutions of nonlinear differential equations. One of the simplest methods is Eulers-method also known as *Forward-Euler*. This method is shown in the pseudo code below

Algorithm 1 Forward-Euler in pseudo code

1: $\mathbf{x_{dd}} = f(\mathbf{x_d}, \mathbf{x})$
2: $\mathbf{x_d}(0) = \mathbf{v_0}$
3: $\mathbf{x}(0) = \mathbf{x_0}$
4: $dt > 0$ *is sufficiently small*
5: **for** $i \leq$ **nr. of iterations ;** $i+ = 1$ **do**
6: $\quad \mathbf{x_{dd}}_{i+1} \leftarrow f(\mathbf{x_d}_i, \mathbf{x}_i)$
7: $\quad \mathbf{x_d}_{i+1} \leftarrow \mathbf{x_d}_i + \mathbf{x_{dd}}_i \cdot dt$
8: $\quad \mathbf{x}_{i+1} \leftarrow \mathbf{x}_i + \mathbf{x_d}_i \cdot dt$
9: **close;**

For computer calculations, round-of errors will increase as $dt \to 0$ [26] [16]. The error of the solution is impossible to eliminate in practice, but for the more precise methods, as *Runge-Kutta 4* and higher order Runge-Kutta-methods, the approximated solution is still a good indicator of how the overall dynamics will behave. The numerical solutions of the different ODEs will approximate the solution within some margin, deviating from the analytical solution for every step. The error rate should be taken into account when these parameters are set. The error for Euler's method for solving the ordinary differential equation, $\dot{x} = f(t, x)$, is given by theorem 13.17 in [26], stated below.

Theorem 13.17

Suppose $f, f_t, f_x \in \mathcal{C}$ are bounded functions on $t \in [a,b]$ and $x \in \mathbb{R}$. Let $\epsilon_k = x(t_k) - x_k$ denote the error at step k, when applying Euler's method with n steps of length h with the condition $x(a) = x_0$. This is described by 2.24

$$|\epsilon_k| \leq h\frac{D}{2C}\big(e^{(t_k-a)C} - 1\big) \leq h\frac{D}{2C}\big(e^{(b-a)C} - 1\big) \tag{2.24}$$

for $k = 0, 1, ..., n$. Where the constants C, D are given by

$$\begin{aligned} C &= \max_{t\in[a,b], x\in\mathbb{B}} |f_x(t,x)|, \\ D &= \max_{t\in[a,b]} |\ddot{x}| \end{aligned} \tag{2.25}$$

where:

$$f_x(t_k, \theta_k) = \frac{f(t_k, x(t_k)) - f(t_k, x_k)}{(x(t_k) - x_k)} \quad \theta_k \in (x_k, x(t_k))$$

The global fault is important for the understanding of the accuracy of the simulation, especially when approaching unstable equilibrium points. The constant C is also known as the *Lipschitz constant* of f [9][11].

2.7 Virtual holonomic constraints

Systems with one or more passive degrees of freedom are called *underactuated* systems. One way to reduce the number of passive DOFs is to introduce physical barriers and/or actuators. For example consider the double pendulum. If the endpoint of the second link is attached to a linear rail, the system loses one passive degree of freedom as the first link and the linear rail describes the position and velocity of the second link. In this example, the linear rail is a *holonomic constraint*. These depend only on positions. A system with multiple passive DOFs can be reduced, even if physical constraints are inactive. A virtual holonomic constraint is a position dependent mathematical relation which, when combined with the equations of motion, reduces the systems number of passive DOFs. Feedback control laws provide the chosen relation between the coordinates [34].

2.8 Motion planning for underactuated system

Given an N-DOF system with one passive degree of freedom r, the desired relation between the coordinate associated with the passive and the non-passive degrees of freedom can be formulated as,

$$q_i = \phi_i(r), \tag{2.26}$$

where i = 1, 2,..., n-1, and

$$\begin{aligned} \dot{q}_i &= \dot{\phi}_i, \\ \ddot{q}_i &= \ddot{\phi}_i. \end{aligned} \tag{2.27}$$

Here r represents the passive coordinate, and q_i represents the $N-1$ non-passive coordinates. The continuously differentiable functions, ϕ_i, are called the *virtual constraints*. Substituting q_i by ϕ_i gives the scalar equation,

$$\alpha(r)\ddot{r} + \beta(r)\dot{r}^2 + g(r) = 0, \tag{2.28}$$

(see [35]), where α, β, g are continuously differentiable functions. Let $r(t)$ be a solution with the initial and end conditions $r(t_0) = r_0$, $\dot{r}(t_0) = \dot{r}_0$, $r(t_1) = r_1$ and $\dot{r}(t_1) = \dot{r}_1$. Then the *integral of motion* or *first integral* (2.29) preserves its zero-value along this solution (see [34]),

$$I(r, \dot{r}, r_0, \dot{r}_0) = \dot{r}^2 - \psi(r_0, r)\Big[\dot{r}_0^2 - \int_{r_0}^{r} \psi(s, r_0)\frac{2\gamma(s)}{\alpha(s)}ds\Big], \tag{2.29}$$

where,

$$\psi(r_0, r_1) = \exp\Big\{-2\int_{r_0}^{r_1}\frac{\beta(\tau)}{\alpha(\tau)}d\tau\Big\}. \tag{2.30}$$

The robot equation with a suggested motion generator can be used in equation 2.29 or the stability and phase portrait of the system can be analyzed using theorem B.1 in section B.1. Substitution of the virtual constraint into the $N-1$ equations associated with active coordinates makes the system of differential equations solvable in terms of the generalized forces. Choice of virtual constraint affects the resulting motion of the passive coordinate.

Chapter 3

Methodology

3.1 Modeling

In this section the different models and modelling approaches for the tripod are presented.

3.1.1 Different coordinate system configurations

In general, there are many possible representations of the different joint angels and positions. The platform on three legs can be considered as a vehicle with NED coordinate system attached to the platform. The scope for this thesis is not to derive control laws in order for the robot to follow a path from one location to another by walking, but rather to find out how walking can be performed. Therefore, coordinate frames more adjusted to this use are preferable. For the tripod, both positions and velocities of the platform and feet, relative to the initial frame at the ground are interesting. A consistent way of describing all joint variables are desirable. Denavit-Hartenberg convention helps provide such coordinates. The figures 3.1 and 3.2 show two different variants. Note that a chain of homogeneous transformations can lead to a long multi-dimensional expression. The coordinate system 3.1 has been briefly analyzed in [29] and it was found to have the D-H table

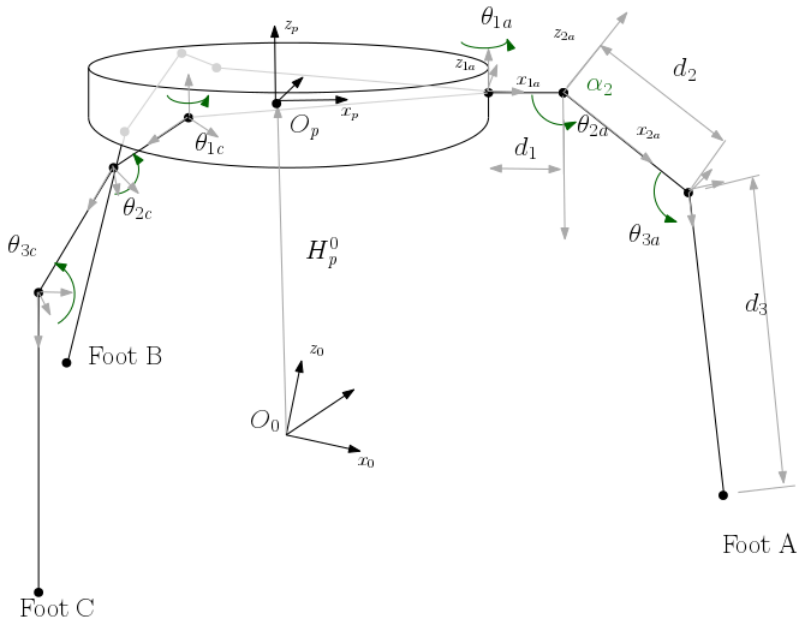

Figure 3.1: Coordinate systems: the initial frame, platform frame.

3.1 for each leg, and a general 6-DOF homogeneous transformation from the initial frame to the platform frame.

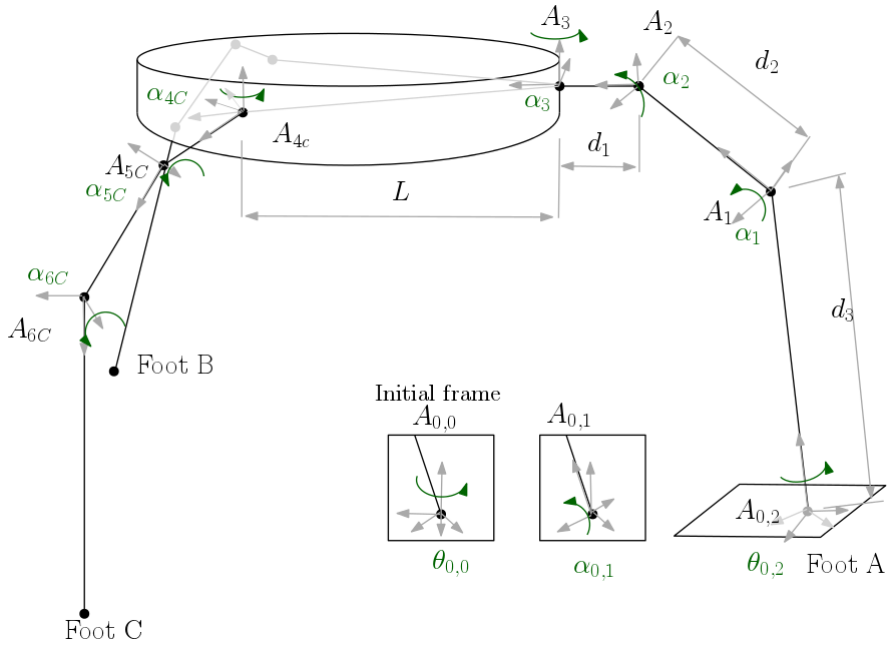

Figure 3.2: Location of the feet coordinate system frames: foot A, foot B, and foot C.

Link	a_i	α_i	d_i	θ_i
0	a_0			θ_{0_i}
1_i	l_1	$-\frac{\pi}{2}$		$\theta^*_{1_i}$
2_i	l_2			$\theta^*_{2_i}$
3_i	l_3			$\theta^*_{3_i}$

Table 3.1: Denavit-Hartenberg table of the complete robot from platform to feet for leg i, from [29]

Link	a	α	d	θ
0.0				$\theta^*_{0.0}$
0.1		$\alpha^*_{0.1}$		
0.2				$\theta^*_{0.2}$
1		α^*_1	d_3	
2		α^*_2	d_2	
3		$\alpha^*_3 + \frac{\pi}{6}$	d_1	$\frac{\pi}{2}$
4_c		$\alpha^*_4 + \frac{\pi}{6}$	L	
5_c		α^*_5	d_2	$-\frac{\pi}{2}$
6_c		α^*_6	d_3	

Table 3.2: Denavit-Hartenberg table of the complete robot from stance leg to feet for leg i

3.1.2 Simple model

Consider a tripod robot with $m_l \ll m_p$[1]. Eliminating the masses and inertials of the legs gives a simplified model compared to the full complexity. This is the simplest model which can still be relevant for a physical implementation. However, the ability to balance when standing on one or two legs is limited. The dynamics of the platform is then described by the forces acting on it, which are gravity and the three forces acting on the hip-platform connection. The symbols used in this section are described in tables 3.3 and 3.4.

[1]Mass of the platform is considerably larger than the leg masses.

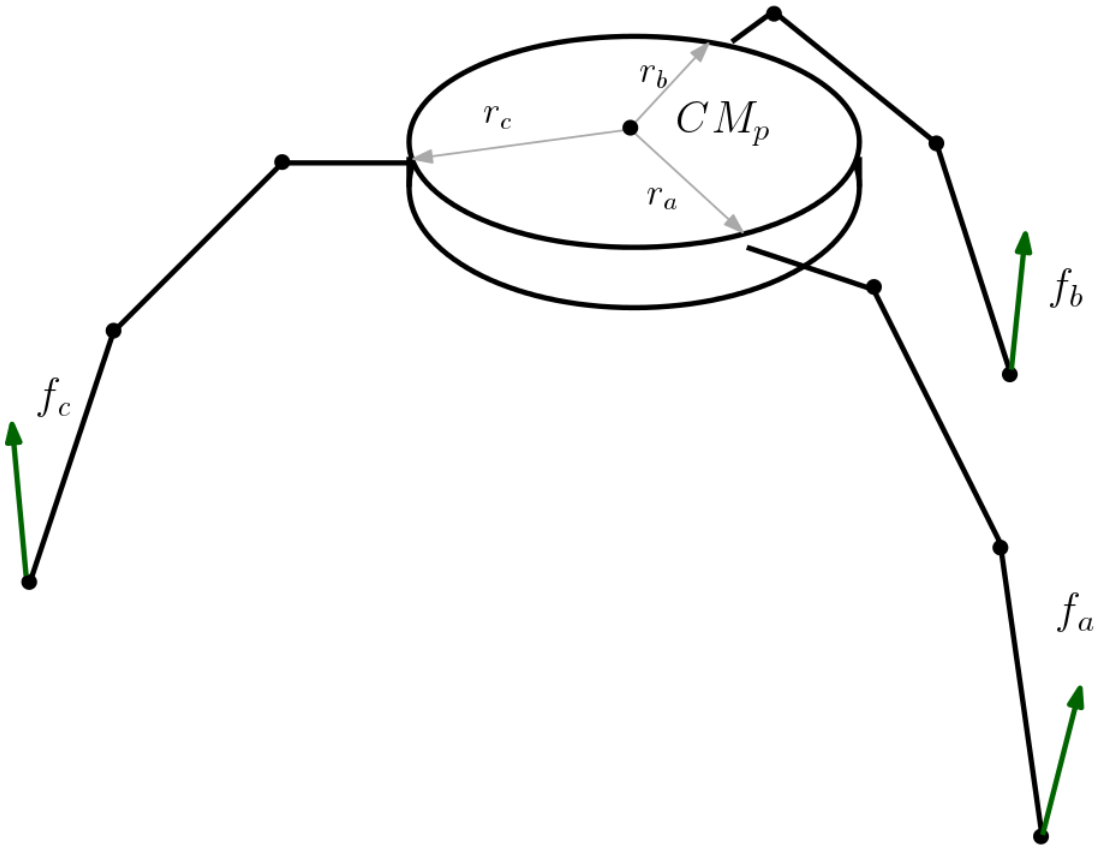

Figure 3.3: External forces acting on the tripod

Symbol	Meaning	Space
m_l	leg-mass	$\mathbb{R}$
m_p, m	platform mass	$\mathbb{R}$
g	Gravitational acceleration	$\mathbb{R}$
O_0	Initial coordinate frame located at ground	$\mathbb{R}^3$
O_p	Platform coordinate frame located at CM of platform	$\mathbb{R}^3$
$\mathbf{F^0_{tot}}$	Total forces acting on platform in O_0	$\mathbb{R}^{3\times1}$
$\mathbf{T^p_{tot}}$	Total torque acting on platform in O_p	$\mathbb{R}^{3\times1}$
$\mathbf{f_a}, \mathbf{f_b}, \mathbf{f_c}$	Forces acting on platform in O_0 at leg attachment points	$\mathbb{R}^{3\times1}$
$\mathbf{r_a}, \mathbf{r_b}, \mathbf{r_c}$	Constant vectors from CM to leg attachment points in O_0	$\mathbb{R}^{3\times1}$
$\mathbf{q_t}, \dot{\mathbf{q}}_\mathbf{t}, \ddot{\mathbf{q}}_\mathbf{t}$	Translatory position, velocity and acceleration in O_0	$\mathbb{R}^{3\times1}$
$\mathbf{q_r}, \dot{\mathbf{q}}_\mathbf{r}, \ddot{\mathbf{q}}_\mathbf{r}$	Angular position, velocity and acceleration in O_p	$\mathbb{R}^{3\times1}$
$\mathbf{I}$	Inertia dyadic of the platform	$\mathbb{R}^{3\times3}$
$\mathbf{T}$	Transformation from hip attachment to foot	$\mathbb{R}^{3\times1}$
$\mathbf{n}$	Normal force on a leg	$\mathbb{R}^{3\times1}$
$\mathbf{f_p}$	Force acting on the platform in a leg attachment point	$\mathbb{R}^{3\times1}$
$\mathbf{f_u}$	Force acting on foot due to desired displacement of CM	$\mathbb{R}^{3\times1}$
$\mathbf{f_o}$	The sum of normal force and .... eh	$\mathbb{R}^{3\times1}$
$\mathbf{\Theta}$	The vector of angular joint positions on a foot	$\mathbb{R}^{3\times1}$

Table 3.3: Description of the variables and parameters in section 3.1.2, and their associated spaces. See figure 3.4 for details on joint parameters and and variables. Part 1

Symbol	Meaning	Space
$\delta\mathbf{\Theta}$	The infinitesimal displacement of the angular joint positions	$\mathbb{R}^{3\times1}$
δA	The virtual work	$\mathbb{R}$
τ	The vector of joint torques	$\mathbb{R}^{3\times1}$
$\mathbf{P}$	Position of foot in O_p	$\mathbb{R}^{3\times1}$
$\delta\mathbf{P}$	The infinitesimal displacement of position of the foot in O_p	$\mathbb{R}^{3\times1}$
$\mathbf{F^p}$	Extended total force vector in platform coordinate frame	$\mathbb{R}^{4\times1}$
$\mathbf{H_p^0}$	The homogeneous transformation from the initial frame, O_0, to the platform frame O_p	$\mathcal{SE}(4)$
d_A, d_B, d_C	Distance from corner A, B, C to the line parallel to the opposing side, intersecting CM	$\mathbb{R}$
h_A, h_B, h_C	Height of the configuration polygon when corner A, B, C is on top	$\mathbb{R}$
$f_{z,A}, f_{z,B}, f_{z,C}$	z-component of the forces acting at the feet	$\mathbb{R}$

Table 3.4: Description of the variables and parameters in section 3.1.2, and their associated spaces. See figure 3.4 for details on joint parameters and and variables. Part 2

First, the motion of the platform due to these forces can be expressed by 3.1 to 3.3 described below, where $\mathbf{F}_{tot}$ describes total force acting on the platform and $\mathbf{T}_{tot}$ describes the resulting torque. This is derived by Newton's second law of motion for rigid body [37], [33]. Hereinafter the superscript notation is used to define the coordinate system frame which the vector is represented in. For example, $\mathbf{F}^0_{tot}$ is the total force acting on the platform written in initial frame, while $\mathbf{T}^p_{tot}$ is the total torque written in the platform frame.
In this notation, the equations of motion of the robot can be written as,

$$\mathbf{F}^0_{tot} = m\ddot{\mathbf{q}}^{\mathbf{0}}_{\mathbf{t}}, \tag{3.1}$$

$$\mathbf{T}^p_{tot} = \mathbf{I}\dot{\mathbf{q}}^{\mathbf{p}}_{\mathbf{r}} + \mathbf{q}^p_r \times (\mathbf{I}\mathbf{q}^p_r), \tag{3.2}$$

$$\frac{d\mathbf{R}}{dt} = (\mathbf{R}\dot{q}^p_r) \times \mathbf{R}, \tag{3.3}$$

where $\mathbf{R}$ is the rotation matrix defining orientation of the platform with respect to the initial frame, $\dot{q}_r^p$ is the angular velocity of the platform given in the platform frame, q_t^0 is the position of the platform given in the initial frame.
The force $\mathbf{F_{tot}^0}$ is just the sum of forces,

$$\mathbf{F}_{tot}^0 = \mathbf{f}_a^0 + \mathbf{f}_b^0 + \mathbf{f}_c^0 + m\mathbf{g},$$

and $\mathbf{T_{tot}^0}$ is the torque acting on the platform induced by these forces,

$$\mathbf{T}_{tot}^0 = \mathbf{P}_a^0 \times \mathbf{f}_a^0 + \mathbf{P}_b^0 \times \mathbf{f}_b^0 + \mathbf{P}_c^0 \times \mathbf{f}_c^0,$$

where,

$$\mathbf{P}_s^p = \mathbf{T}_s^p(\mathbf{\Theta}) + \mathbf{r}_s^p,$$

is the position vector of feet $s \in \{a, b, c\}$ in platform frame. For a leg, this vector $T^p(\theta_1, \theta_2, \theta_3)$ can be found geometrically (see figure 3.4)

$$\mathbf{T^p} = \begin{bmatrix} (d_1 + d_2\cos\theta_2 + d_3\cos(\theta_2 + \theta_3))\cos\theta_1 \\ (d_1 + d_2\cos\theta_2 + d_3\cos(\theta_2 + \theta_3))\sin\theta_1 \\ -(d_2\sin\theta_2 + d_3\sin(\theta_2 + \theta_3)) \end{bmatrix}. \tag{3.4}$$

To investigate how associated motor torques $\tau_\mathbf{i}$ influence the platform forces $\mathbf{f}$, the D'Alembert's principle of virtual work is used. In figure 3.4, $\mathbf{n}$ is the normal force at the foot, $\mathbf{f}_u$ is the tangential component of the force, and $\mathbf{f}_0$ is the sum of these forces, i.e. the total force acting on the foot[2]. To express the force f through motor torques τ_i and angles θ_i, consider a small displacement δP of a leg influenced by this force. Within this displacement the angles θ_i were changed by $\delta\theta_i$, then the total work of the force, f, is equal to

$$\begin{aligned} \delta A &= \sum_{i=1}^{3} \tau_i \cdot \delta\theta_i \\ &= \tau^T \cdot \delta P. \end{aligned}$$

Taking into account that,

$$\delta P = \sum_{i=1}^{3} \frac{\partial P}{\partial \theta_i} \delta\theta_i,$$

[2]The friction between the ground surface and the foot is considered sufficiently large, preventing sliding.

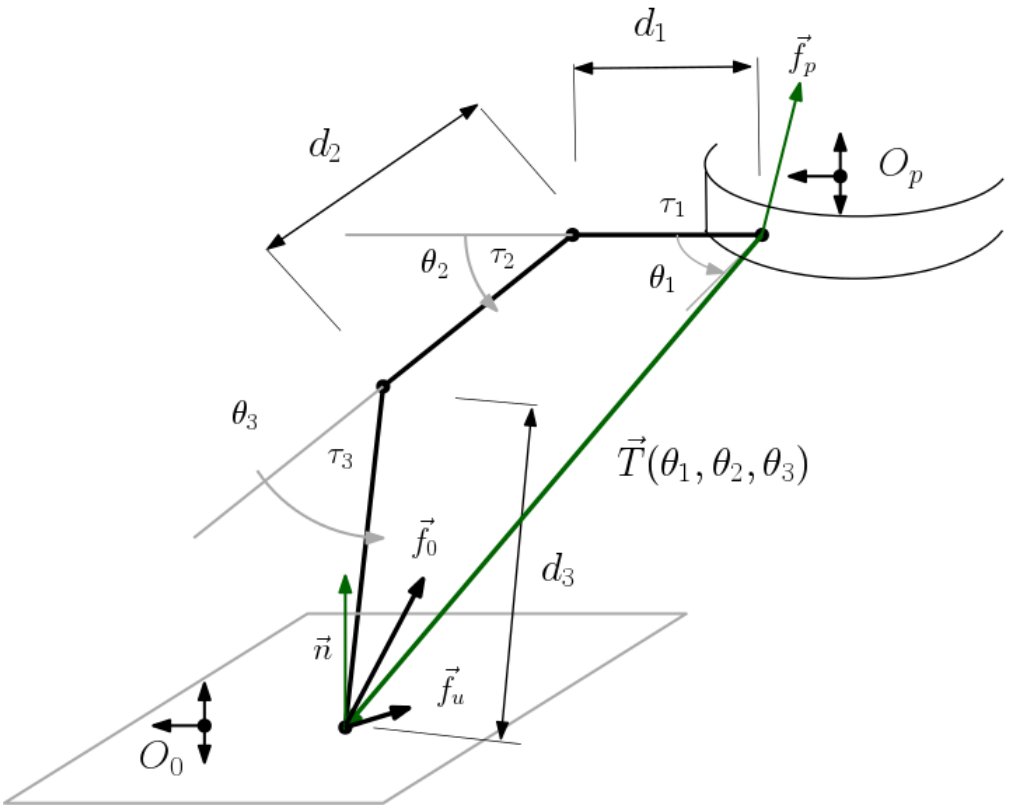

Figure 3.4: Transformation vector from hip-platform connection to feet

will have,

$$\tau_i = f^T \frac{\partial P}{\partial \theta_i}, \tag{3.5}$$

the Jacobian $\frac{\partial P}{\partial \theta_i}$ in equation 3.5 becomes a matrix in $\mathbb{R}^{3\times 3}$:

$$\frac{\partial \mathbf{P}}{\partial \mathbf{\Theta}} = \begin{bmatrix} -s\theta_1(d_1 + d_2c\theta_2 + d_3c(\theta_2+\theta_3)) & c\theta_1(-d_2c\theta_2 + d_3c(\theta_2+\theta_3)) & -c\theta_1(d_3s(\theta_2+\theta_3)) \\ c\theta_1(d_1 + d_2c\theta_2 + d_3c(\theta_2+\theta_3)) & s\theta_1(-d_2c\theta_2 + d_3c(\theta_2+\theta_3)) & -s\theta_1(d_3s(\theta_2+\theta_3)) \\ 0 & -d_2c\theta_2 - d_3c(\theta_2+\theta_3) & -d_3c(\theta_2+\theta_3) \end{bmatrix} \tag{3.6}$$

Here $\mathbf{P} = \mathbf{P}^p$ is the position of the foot from center of the platform. The radius vector $\mathbf{r}$ is a constant.

Note that notations for sine and cosine are simplified in the matrix in equation 3.6. The torques in equation 3.5, are expressing the force acting on the foot due to both movement of the platform and gravity. In equation 3.8, the extended force vector in the initial frame is expressed as the product between the homogeneous transformation from the initial frame to the platform frame, and this force vector in the platform frame shown below,

$$\mathbf{F^P} = \begin{bmatrix} \mathbf{f} \\ \mathbf{0} \end{bmatrix}, \tag{3.7}$$

$$\mathbf{F^0} = \mathbf{H_p^0 F^P}. \tag{3.8}$$

The relation between position of the platform, the position of the feet, and the normal forces in the initial frame gives us the missing information needed in order to complete the dynamic model. The size of normal force for each leg is dependent on the position of center of mass of the robot and the configuration polygon. In figure 3.5, the distances d_I describe the distance from the center of mass to corner I, parallel to the line running through corner I and being orthogonal to the opposite side. This distance, h_I, is the height of the triangle. Note that in this case the configuration polygon is considered orthogonal to the gravity vector[3]. From this,

[3]Projection might be useful for analysis if otherwise

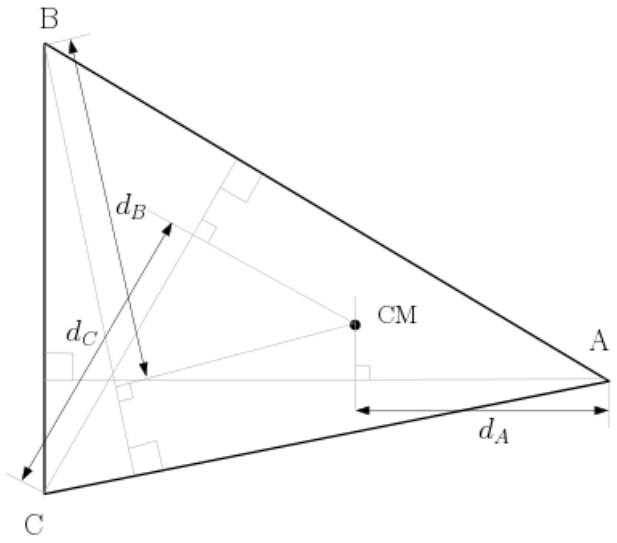

Figure 3.5: Configuration polygon with CoP located on the inside

one can derive the forces acting on each foot in the direction parallel to gravity. As there is nothing keeping the feet on ground, such as attracting forces between feet and ground, the force at each foot will always be less or equal to zero, when positive direction is defined to be the opposite of the direction of the gravity vector. Described mathematically,

$$f_{z,A} = \begin{cases} mg(1 - \frac{d_A}{h_A}) & \text{if } d_A < h_A \\ 0 & \text{if } d_A \geq h_A \end{cases}. \tag{3.9}$$

Here, foot A is used as an example.

A direct result of this, is that one way to lift a leg is to move the center of pressure (CoP) outside of the configuration polygon. Even for models which include the link masses for the legs, this will be true. However, the position of CM and therefore CoP depends on the joint variables in those cases.

3.1.3 The Euler-Lagrange models

The full complexity Euler-Lagrange model for the the tripod using the generalized coordinates showed in the tables 3.1 and 3.2 are not present in this report. The two approaches gave 15 and 12 equations respectively . These were calculated analytically using MATLAB R2018a and written to a text document. The 15 equations derived in [29] are not practical in their symbolic form, and the 12 equations gained from the same program[4] is also extensive beyond practicalities as symbolic equations. Simplifying the parameters such as mass, inertia and lengths of different legs, setting them equal to one, simplifies the equations. The main contribution to the size of the formulas are dimensions. The links described by a long chain of homogeneous transformations become high dimensional expressions.

[4]The MATLAB code was extensively reimplemented to fix minor bugs and increase readability in conjunction with this work.

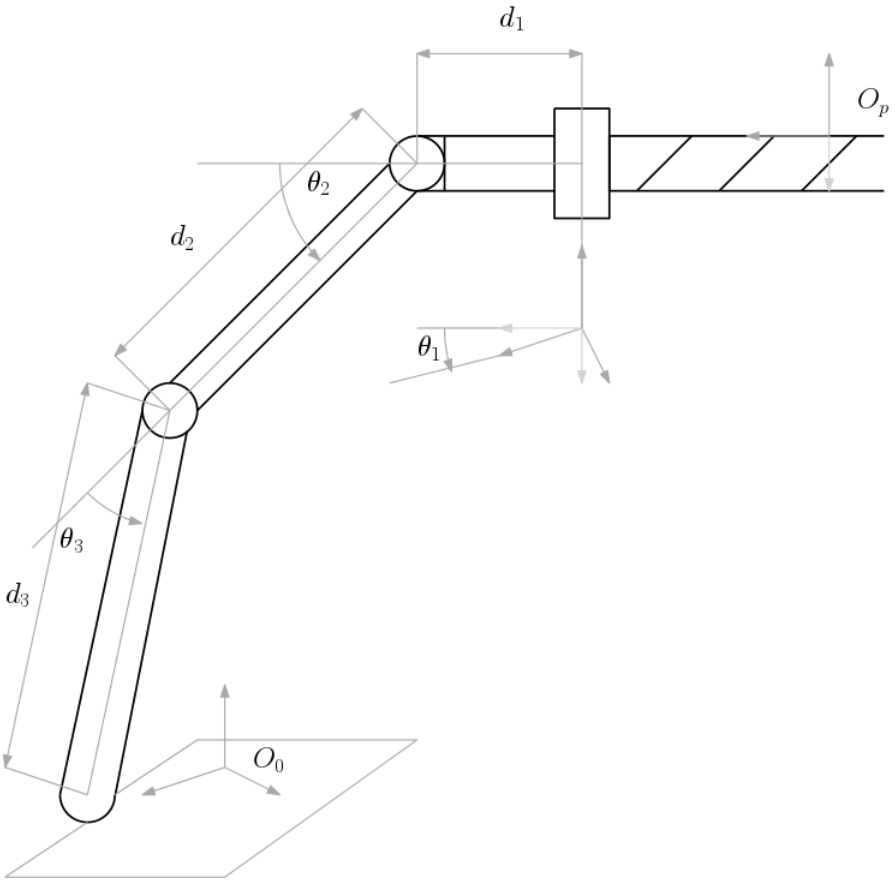

Figure 3.6: Leg when platform mass >> leg mass

The Euler-Lagrange model of one leg attached to a stiff platform with $m_p >> m_l$, consists of three generalized coordinates viewed in table 3.1. The equations can be written in the standard matrix form viewed in equation 2.15. Note that the z-axis of the platform frame, O_p is aligned with the gravity vector in the equations,

$$D = \begin{bmatrix} \Psi & i_2\cos^2(\theta_2) + i_3\cos^2(\theta_3) & i_3\cos^2(\theta_3) \\ i_2\cos^2(\theta_2) + i_3\cos^2(\theta_3) & i_2\cos^2(\theta_2) + i_3\cos^2(\theta_3) & i_3\cos^2(\theta_3) \\ i_3\cos^2(\theta_3) & i_3\cos^2(\theta_3) & i_3\cos^2(\theta_3) \end{bmatrix}, \quad (3.10)$$

Symbol	Meaning	Space
D	Inertia matrix	$\mathbb{R}^{3\times3}$
C	Coriolis matrix	$\mathbb{R}^{3\times3}$
$\mathbf{g}$	Gravity terms	$\mathbb{R}^{3\times1}$
m_i	Mass of link i	$\mathbb{R}$
g	Gravitational acceleration	$\mathbb{R}$
d_i	Length of link i	$\mathbb{R}$
i_j	Inertias associated with link j	$\mathbb{R}$
θ_i	Angles as indicated in figure 3.6	$\mathbb{R}$
τ_i	Torques associated with joints	$\mathbb{R}$

Table 3.5: Description of the symbols in the matrix 3.10 and the gravity vector 3.13

where,

$$\begin{aligned}\Psi &= i_1\cos^2(\theta_1) + i_2\cos^2(\theta_2) + i_3\cos^2(\theta_3) + d_2^2 m_2\cos^2(\theta_2)\\ &+ d_2^2 m_3\cos^2(\theta_1) + d_3^2 m_3\cos^2(\theta_1) + d_2^2 m_2\sin^2(\theta_1)\\ &+ d_2^2 m_3\sin^2(\theta_1) + d_3^2 m_3\sin^2(\theta_1) + 2d_2 d_3 m_3\cos^2(\theta_1)\\ &+ 2d_2 d_3 m_3\sin^2(\theta_1),\end{aligned} \tag{3.11}$$

$$C = \begin{bmatrix} -i_1\cos(\theta_1)\sin(\theta_1)\dot{\theta_1} & -2i_2\cos(\theta_2)\sin(\theta_2)\dot{\theta_2} & -2i_3\cos(\theta_3)\sin(\theta_3)\dot{\theta_3}\\ i_2\cos(\theta_2)\sin(\theta_2)\dot{\theta_1} & -i_2\cos(\theta_2)\sin(\theta_2)\dot{\theta_2} & -2i_3\cos(\theta_3)\sin(\theta_3)\dot{\theta_3}\\ i_3\cos(\theta_3)\sin(\theta_3)\dot{\theta_1} & i_3\cos(\theta_3)\sin(\theta_3)\dot{\theta_2} & -i_3\cos(\theta_3)\sin(\theta_3)\dot{\theta_3}, \end{bmatrix} \tag{3.12}$$

and,

$$\mathbf{g} = \begin{bmatrix} 0\\ \frac{g}{2}\big(d_3 m_3\sin(\theta_2)sin(\theta_3) + d_3 m_3\cos(\theta_2)\cos(\theta_3) - d_2 m_2\cos(\theta_2)\big)\\ \frac{d_3 g m_3}{2}\big(\sin(\theta_2)\sin(\theta_3) - \cos(\theta_2)\cos(\theta_3)\end{bmatrix}. \tag{3.13}$$

In equations 3.10 to 3.13 a few simplifications are made for practical reasons. The

inertia matrices for each link are $[i_k I^3, \quad k = 1, 2, 3]$, where i_k is a constant and I^3 is the identity matrix of dimension 3. The position of centers of mass of each leg is located on the middle of the link.

The robot equation in matrix form hence becomes,

$$D(\theta)\ddot{\theta} + C(\theta, \dot{\theta})\dot{\theta} + \mathbf{g}(\theta) = \begin{bmatrix} \tau_1 \\ \tau_2 \\ \tau_3 \end{bmatrix}. \tag{3.14}$$

Note that the passive variant of the first equation in 3.14 has an equilibrium at $\theta_1 = 0$, since the gravity vector 3.13 has a zero in its first row.

To express the leg equations more generally, adding realistic link inertia matrices and adjusting the orientation of the platform, and hence the direction of the gravity vector, can easily be done with slight modifications to the Matlab script called *leg_movement_calculation.m*.

3.1.4 Simplified and semi-simplified model of tripod during two-leg stance

The simplest model form of the tripod dynamics while in two-leg stance, is an inverted pendulum with adjustable length, as depicted in figure **??**. This robot has one passive degree of freedom, ϕ_1. Naturally, other joint variables, as the hip angles, will introduce different possible motions for the robot, but the lack of mass makes it impossible for it to balance. The forces due to movement of the legs simply do not affect the platform dynamics, if its not connected to the normal forces from the feet. Hence, further investigation of this model will not be included in this report.

The simplified equations of motion for this system is described in equations 3.15 to 3.18. Even if balancing is impossible for the simple model, it can still be used to find gaits.

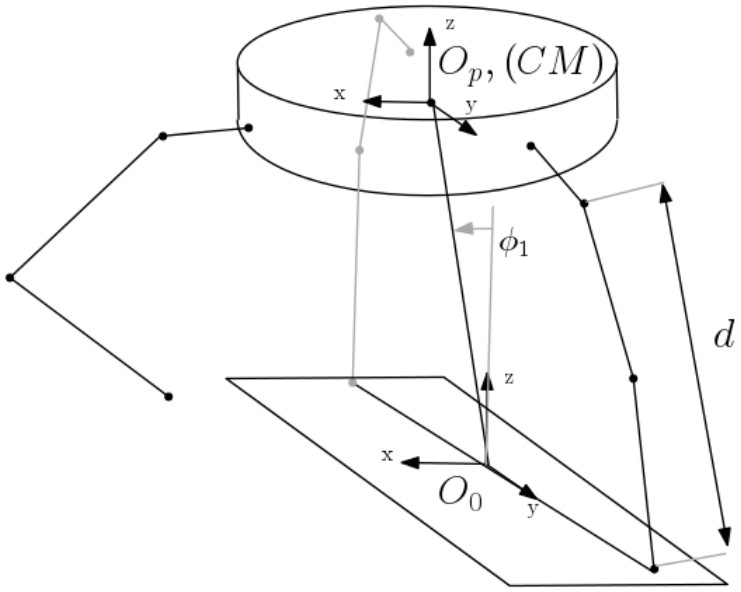

Figure 3.7: Leg when platform mass >> leg mass

$$P = mgd\cos\phi_1 \tag{3.15}$$

$$K = \frac{1}{2}m(\dot{d}^2 + \dot{\phi}_1^2 d^2) \tag{3.16}$$

$$m\ddot{d} + gm\cos\phi_1 - md\dot{\phi}_1^2 = f(\tau) \tag{3.17}$$

$$md^2\ddot{\phi}_1 + 2md\dot{d}\dot{\phi}_1 - gmd\sin\phi_1 = 0 \tag{3.18}$$

As mentioned in the beginning of this section, the full Euler-Lagrange model based on the D-H tables in section 2.3, leads to an amount of symbolic expressions unfit for symbolic analysis. Intuition suggests introduction of mass for the leg-links would make balancing on two legs possible for the tripod. A semi-simplified model where some point masses are included are therefore needed. Note that balancing is not necessary for gaits, but the property permits a huge variety of strategies. The aim is to develop a relevant[5] model for developing gaits. The two dimensional model where θ_1 is fixed such that the rotational axis of knees are parallel has been described in great detail [12].

[5]Less realistic models can still be relevant. Often complexity of models are reduced considerably in similar projects. One example is [17]

Symbol	Meaning	Field
P	Potential energy	$\mathbb{R}$
K	Kinetic energy	$\mathbb{R}$
m	Mass of platform	$\mathbb{R}$
g	Gravitational acceleration	$\mathbb{R}$
d	length of the inverted pendulum	$\mathbb{R}$
ϕ_1	Angle as indicated in figure 3.7	$\mathbb{R}$

Table 3.6: Description of the symbols in equations 3.16 to 3.18

A general fact when constructing robots with long links and heavy motors, is that motors and other heavy components should not be placed far out on a swinging arm. This is to reduce needed torque of the motors or other actuators. During the design of the physical tripod in [30], this was considered. As shown in [4] and other projects, gears and belts can be used to displace the mass, however these methods have limitations too. The motors controlling the hip-links do not move considerably for the tripod, because of the in principle shorter hip-link. These masses are reasonable to eliminate in a simplified model. However, the motors actuating the outer leg-link is placed at the knee, and will affect the center of mass and inertia considerably.

For simplicity the model will be considered in 2-D, with no rotation of the platform in the z or x axis. As before, this forces the stance-leg variables to be symmetric. Firstly, assume the hip-joint variables of the stance legs θ_{1A}, θ_{1B} are fixated. Due to the friction between the feet and the ground surface, assumed to always be sufficiently large to prevent sliding, sideways motion of the free leg, in this case leg C, will not introduce rotation of the platform[6]

The model is similar to the the one shown in figure 3.8 and the equations become 3.19 and 3.20[7].

The passive coordinates for this system is $\alpha_{0,0}$ shown in figure 3.2, which is a good

[6]The stance-leg joint torques must oppose this torque, but this will not be addressed further.

[7]The $\aleph$ in these equations represent α in the scalar robot equation 2.28

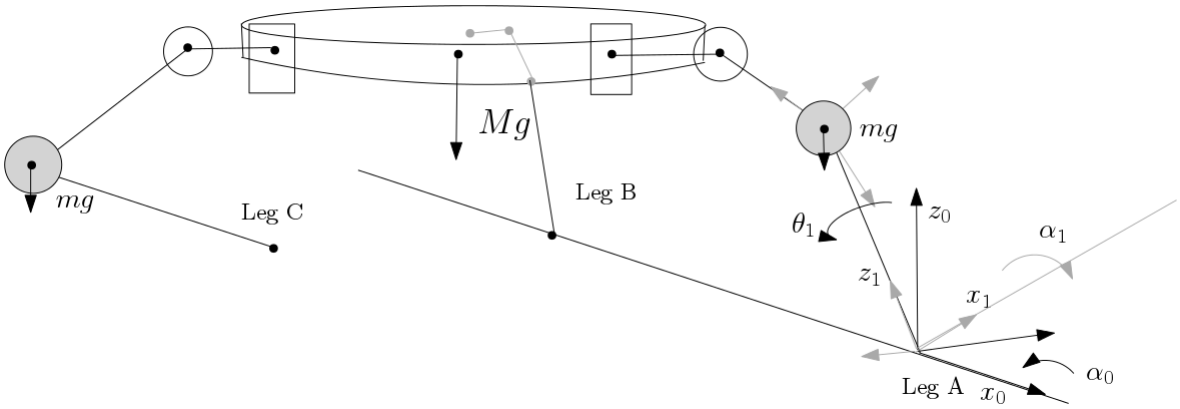

Figure 3.8: The semi-simple model includes masses on knees based on 3.2

coordinate representation because of the relation to the angle on the ground surface. However, it is known that the center of mass of the robot will rotate about the line spanned between the two feet. Hence, slight modifications should be made. The modifications can be seen in figure 3.8. The generalized coordinate α_0 is in a more direct way connected to the line between feet A and B. This is now the coordinate associated with the passive dynamics. Note that this representation is equivalent to the one depicted by table 3.2.

$$\aleph(\alpha_0)\ddot{\alpha}_0 + \beta(\alpha_0)\dot{\alpha}_0^2 + \gamma(\alpha_0) + f(\ddot{\mathbf{q}}/\ddot{\alpha}_0, \dot{\mathbf{q}}/\dot{\alpha}_0, \mathbf{q}/\alpha_0) = 0 \tag{3.19}$$

$$\aleph(q)\ddot{q} + \beta(q, \dot{q})\dot{q} + g(q) = f(\tau) \tag{3.20}$$

All the other generalized coordinates are related to a joint torque or a combination of joint torques. Note that the constraint due to symmetry of the support legs makes θ_1 dependent on the other joint variables. To analyze the phase-portrait of this system, some values must be fixated.

A similar approach depicted in figure 3.9, where all leg-joint frames are equivalent to the ones depicted in table 3.1, can be more compact. Here, the coordinate representing the passive dynamics is ϕ_0. Both the angle of the platform and the length l_0 can be derived by the other joint variables on the support-legs. The vector

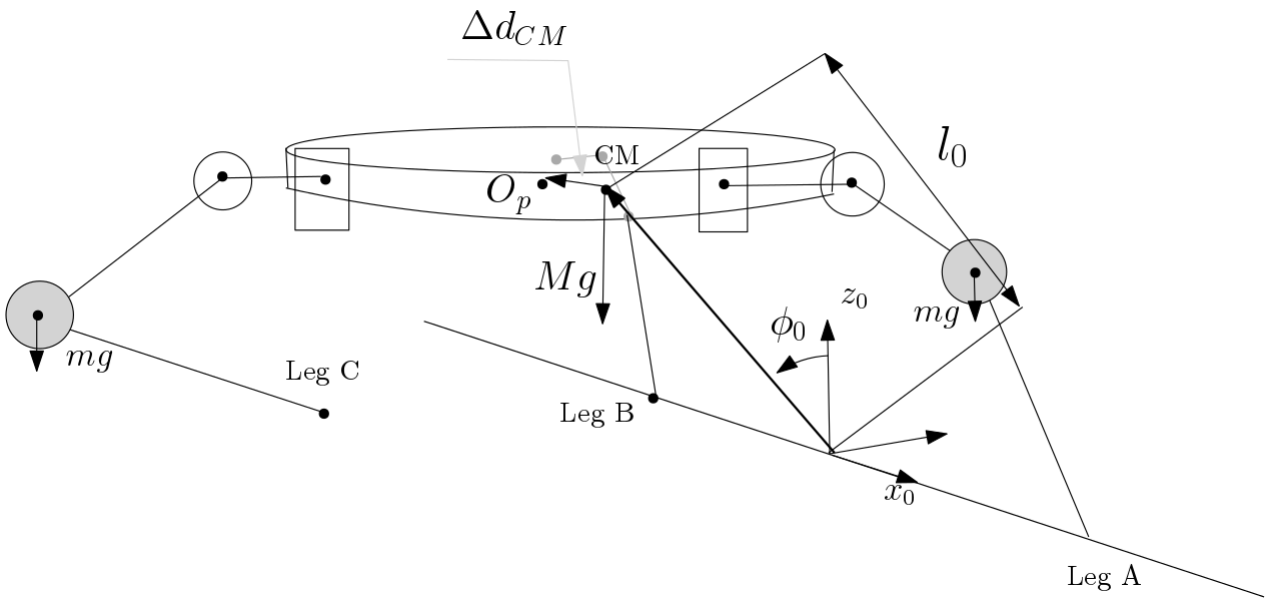

Figure 3.9: The semi-simple model includes masses on knees based on 3.2 and 3.1

function describing the distance between the center of the platform and the CM can be derived using more accurate models, including masses for each link, and will depend only on the joint parameters. As the initial coordinate system is placed on the symmetry line between the two support-legs, a two-dimensional analysis is desirable.

Symbol	Meaning	Field
$\star/*$	The set $\star$ except the element(s) $*$	$\star$
α_0	The passive degree of freedom in 3.8	$\mathbb{R}$
M	Mass of platform	$\mathbb{R}$
m	Mass of knees	$\mathbb{R}$
g	Gravitational acceleration	$\mathbb{R}$
d_i	Length of link i	$\mathbb{R}$
l_0	Length of the inverted pendulum	$\mathbb{R}$
ϕ_0	Generalized coordinate for system3.9	$\mathbb{R}$
Δd_{CM}	vector from CM to center of platform	$\mathbb{R}^3$
CM^p	Center of mass in platform frame	$\mathbb{R}^3$
O_p	Center of platform in platform frame	$\mathbb{R}^3$
$H^{j,i}_{j,k}$	The homogeneous transformation from frame i to k for leg j	$\mathbb{R}^{4\times4}$

Table 3.7: Description of the symbols in equations 3.19 to 3.23

For the position angle ϕ_1 and the length l_0 to be calculated correctly, the position of center of mass is crucial. If $\Delta d_{CM} = \mathbf{0}$ in the model, the coordinates ϕ_1 and l_0 are generalized coordinates which can give descriptive intuition as long as the CM is close to the center of the platform, O_p. If however Δd_{CM} is given by the vector in equation 3.21, the generalized coordinates ϕ_1 and l_0 become key elements regarding the intuitive understanding of the system. This is shown by,

$$\Delta d_{CM} = O_p - CM^p(\mathbf{q}), \tag{3.21}$$

$$CM^p(\mathbf{q}) = \frac{1}{M+3m}\Big(\sum_{i=a,b,c}^{3} m_i H^p_{i,2}\,[d_2,0,0]^T\Big), \tag{3.22}$$

where,

$$= \frac{m}{M+3m}\big(H^p_{a,1}H^{a,1}_{a,2} + H^p_{b,1}H^{b,1}_{b,2} + H^p_{c,1}H^{c,1}_{c,2}\big)[d_2,0,0]^T. \tag{3.23}$$

As the homogeneous transformations in 3.23, equivalently to those in 3.1, are dependant on joint variables, Δd_{CM} is a six-dimensional function of positions. Hence,

ϕ_1 and l_0 depend on these additional variables. Similarly, for a generalized version, where all the link masses are included, these functions will depend on all the joint variables.

3.1.5 Impact models

In this section, impact for the tripod is briefly presented as an introductory part only. This report will not derive different impact models for the tripod in detail. It is however a reasonable task for the future. The different responses due to impact for the tripod is crucial for gait design. First consider the simplest version of the impact model, namely the perfectly inelastic model. For any impact where a swing leg hits the ground, the velocity will instantly become equal to zero. Gaits based on this model will include a stage where the robot lifts the leg without the impulse-generated velocities on feet. Even if the impulse forces acting on the colliding leg parallel with the normal force is equal to zero, the moving masses elsewhere on the tripod can lead to rolling, and yield instantaneous switching of stance. Assuming that there is at least one leg on the ground at any time, the table 3.8 describes the different outcomes. Note that the indexing of each leg is not fixed.

Number	Initial stance	Stance when colliding	Resulting stance
1	Two-leg	Three-leg	Three-leg
2	Two-leg, (A,B)	Three-leg	Two-leg, (A,B)
3	Two-leg, (A,B)	Three-leg	Two-leg, (A⊕B,C)
4	Two-leg, (A,B)	Three-leg	One-leg (C)
5	Two-leg, (A,B)	Three-leg	One-leg (A⊕B)
6	One-leg	Three-leg	Three-leg
7	One-leg, (A)	Three-leg	Two-leg, (B,C)
8	One-leg, (A)	Three-leg	Two-leg, (A,C⊕B)
9	One-leg, (A)	Three-leg	One-leg, (A)
10	One-leg, (A)	Three-leg	One-leg, (B⊕C)
11	One-leg, (A)	Two-leg, (A, B⊕C)	One-leg, (A)
12	One-leg, (A)	Two-leg, (A, B⊕C)	One-leg, (A)

Table 3.8: Overview of the different outcomes of impact for the tripod. ⊕ indicates exclusive or.

3.1.6 Impact models on Lagrange-form

For the tripod, the method indicated in 2.5 can be implemented. It is usual to assume no sudden change in positions at impact, and that the tripod is a rigid solid. To keep track of the velocities of the feet, additional coordinates describing these positions are added to the state vector such that the extended vector of coordinates are described by $\mathbf{q}_e$. The models then become on the form,

$$D_e(\mathbf{q_e}^+)\dot{\mathbf{q}}_\mathbf{e}^+ - D_e(\mathbf{q_e}^-)\dot{\mathbf{q}}_\mathbf{e}^- = F_{ext}, \tag{3.24}$$

$$\tag{3.25}$$

with D_e from 2.15, which denotes the conservation of momentum [12][19].
The expanded velocity vector $\dot{\mathbf{q}}_\mathbf{e}^-$ consists of the velocities an infinitesimal moment before impact. These velocities are known, and hence the velocities just after impact $\dot{\mathbf{q}}_\mathbf{e}^+$ can be calculated. The assumption implies that $\mathbf{q_e}^+ = \mathbf{q_e}^-$. Using the principle of virtual work one can describe the external forces by relation 3.26

$$F_{ext} = \frac{\partial P_e}{\partial \mathbf{q_e}} F_{feet} \tag{3.26}$$

where F_{feet} is the forces acting at the swing leg(s)

In 3.26, P_e denotes the positions of the feet in Cartesian coordinates. Using the non-slip assumption leads to the final relation necessary to represent the model as,

$$\frac{\partial P_e}{\partial \mathbf{q_e}} \dot{\mathbf{q}}_\mathbf{e}, \tag{3.27}$$

The compressed form become,

$$\begin{bmatrix} D_e(\mathbf{q_e}^-) & \frac{\partial P_e}{\partial \mathbf{q_e}} \\ \frac{\partial P_e}{\partial \mathbf{q_e}} & \mathbf{0} \end{bmatrix} \begin{bmatrix} \dot{\mathbf{q}}_\mathbf{e}^+ \\ F_{ext} \end{bmatrix} = \begin{bmatrix} D_e(\mathbf{q_e}^-)\dot{\mathbf{q}}_\mathbf{e}^- \\ \mathbf{0} \end{bmatrix}. \tag{3.28}$$

Note that the elasticity in equation 2.22 is equal to zero in this equation due to the assumption.

3.2 Design of motions for the tripod

3.2.1 Repositioning of a single leg

The motions and models in this report are focused on a few situations. The three-leg stance where the platform moves, and the configuration polygon, is fixated in the initial frame, O_0, and the two-leg stance, where the swing leg is lifted from the ground. In figure 3.10, the different alternatives for a new CP. Based on these shown types of steps, several combinations in a sequence can be functioning strategies of walking. Note that the repositioning, D, in figure 3.10, describes the situation where one leg is placed between the two stance legs. The repositioning marked by A will be most important in this thesis, however B and C are closely related, considering the simple model, and also due to sufficient friction forces preventing slipping even if the swing leg leads to roll-torque.

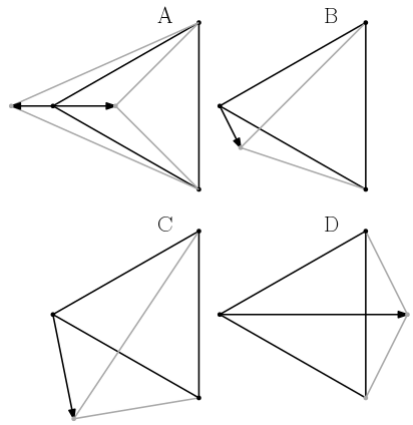

Figure 3.10: Overview of four different ways of repositioning the swing leg. The gray lines indicated the next position.

3.2.2 Analysis of configuration space and trajectories

The configuration space of the tripod is dependant on the type of stance [8] and the configuration polygon. As stated in [38], singularities in configuration space can become serious considerations for three-legged platforms. In this context the singularities are due to sudden loss of DOFs in task-space or if the task frame, the platform, are able to move although actuators are locked. Considering the contact points on ground as attached points able to rotate freely in addition to and passive hip joints, singularities in terms of sudden loss and gain of degrees of freedom can be problematic, and must be avoided [39][38]. As the joints are actuated this is not a problem for the tripod. Note that such eventual problems could arise if inaccuracy in the motors lead to opposing forces greater than the torques of an individual motor, and if slack in the motors is prominent. When standing on a flat surface, this is unlikely due to the friction forces that are not infinite in reality. For simulation purposes, implementation of friction can solve such eventual problems.

Even if the joint variables follow a trajectory $T(\Theta)$ within the configuration space of the tripod, desired motion can be unstable, as shown in [6]. Hence, the sufficient

[8] three, two or one-leg stance.

conditions described in Appendix B.1 with equation B.1 is used.
Considering the foot following a trajectory $T(\Theta)$, the robot equation on matrix form, 2.15, for the system is now with the trajectory $T(\Theta)$ expressed as generalized forces.

The following part addresses this case, one leg at a time. The configuration space is easily described by putting the upper and lower limits for each angle in the transformation 3.4. Assuming trajectories are possible to realize for an under-actuated dynamical system, can be risky, although it might seem trivial, as indicated by [6]. However, the insect-leg is fully actuated[9], such that the motion planning problem becomes an inverse kinematic problem.

Assuming the platform is moving perpendicular to the line between leg A and B, as indicated in figure 3.11, with constant height, and with the platform orientation equivalent to the initial frame,[10] the trajectory for leg A must follow the constraints,

$$A_1A_2A_3\begin{bmatrix} d_3 \\ 0 \\ 0 \\ 1 \end{bmatrix} \cdot [1,0,0,0] = c_1, \quad c_1 \in \mathbb{R}, \tag{3.29}$$

$$T - T_0 \perp A - B \tag{3.30}$$

$$\left|(O_p\mathbf{r_a} - T) \cdot [1,0,0,0]\right| = c_2, \quad c_2 \in \mathbb{R}. \tag{3.31}$$

Inspecting the transformation 3.4, which is based on the same coordinate frames, constraint 3.29 becomes,

$$-(d_2 sin\theta_2 + d_3 sin(\theta_2 + \theta_3)) = c_1. \tag{3.32}$$

Likewise, constraint 3.31 becomes,

$$|(d_1 + d_2\cos\theta_2 + d_3\cos(\theta_2 + \theta_3))\cos\theta_1| = c_2. \tag{3.33}$$

[9]The three joints have actuators for each DOF
[10]This allows us to use the model described in section 3.1.3

To move the foot backwards relative to the platform, the inequality below is sufficient,

$$\frac{d}{dt}[(d_1 + d_2\cos\theta_2 + d_3\cos(\theta_2+\theta_3))\sin\theta_1] < 0. \tag{3.34}$$

The parametrization of a straight line by the generalized coordinates of the insect leg becomes,

$$r_{x,y} = d_1 + d_2\cos\theta_2 + d_3\cos(\theta_2+\theta_3), \tag{3.35}$$

$$r_{x,y}(\theta_1) = \frac{x_0}{\cos(-\theta_1)}, \tag{3.36}$$

$$d_2\sin\theta_2 + d_3\sin(\theta_2+\theta_3) = z_0. \tag{3.37}$$

Hence we get,

$$\theta_3 = \sin^{-1}\big(\frac{-d_2\sin\theta_2 - z_0}{d_3}\big) + 2\pi n - \theta_2, \quad n \in \mathbb{Z}. \tag{3.38}$$

$$\tag{3.39}$$

Inserting the expression for θ_3 in the equation of θ_2 and θ_1 gives,

$$\frac{x_0}{\cos -\theta_1} = d_1 + d_2\cos\theta_2 + d_3(\cos\theta_2\cos\theta_3 + \sin\theta_2\sin\theta_3), \tag{3.40}$$

where

$$\begin{aligned}\cos\theta_3 &= \Big(1 - \big(\frac{d_2\sin\theta_2 - z_0}{d_3}\big)^2\Big)^{\frac{1}{2}}\cos\theta_2, \\ &+ \big(\frac{-d_2\sin\theta_2 - z_0}{d_3}\big)\sin\theta_2, \end{aligned}\tag{3.41}$$

$$\begin{aligned}\sin\theta_3 &= \big(\frac{-d_2\sin\theta_2 - z_0}{d_3}\big)\cos\theta_2, \\ &- \Big(1 - \big(\frac{d_2\sin\theta_2 - z_0}{d_3}\big)^2\Big)^{\frac{1}{2}}\sin\theta_2. \end{aligned}\tag{3.42}$$

Using *MapleSoft* to get an expression of 3.40 in terms of θ_1 gives an extensive expression. However, this can be numerically solved, and used for the motion of the leg.

Parametrization of the back leg, C, with $\theta_{1c} = 0$ gives the equations,.

$$d_1 + d_2 \cos\theta_2 + d_3 \cos(\theta_2 + \theta_3) = x_0 - f(t), \tag{3.43}$$

$$-(d_2 \sin\theta_2 + d_3 \sin(\theta_2 + \theta - 3)) = -z_0 \tag{3.44}$$

$$\theta_3(t) = \frac{\theta_{3_0}}{t_1 - t} - \frac{\theta_{3_1}}{t_1} t, \tag{3.45}$$

where t_1 is stop and

$$\theta_2 + \theta_3(t) = \arcsin\Big(\frac{-(z_0 + d_2 \sin(\theta_2))}{d_3}\Big). \tag{3.46}$$

Equation 3.46 can be solved for θ_2. Note that this is only one particular parametrization and other parametrizations might be better for this motion.

3.2.3 Movement of platform during three-leg stance using simplified model

For the simple model developed in section 3.1.2, there are several two-legged gaits, where one leg moves at a time. In order to move the leg without needing a friction model, there are two main strategies which can work for general models of the tripod. Either the CoP can move outside of the CP, or the moving leg can start by kicking off without adjusting the CoP's position relative to the CP. The former strategy has some requirements on the leg lengths and geometry of the CP. A special case of the latter is that a leg can also simply be lifted, and put down if the actuators are fast enough. Firstly the dynamics on moving the CoP within the CP are described by equation 3.9.

A force acting on the platform in the direction towards the middle of one of the sides of the CP will induce a movement as depicted in figure 3.11. For simplicity, consider the orientation of the reference frames of the platform and the floor perpendicular to the front line of the CP, and the z-axis pointing in the direction opposite to gravity. The initial CP is considered being an equilateral triangle. Equations 3.47 to 3.49 describe the properties of the constant platform vectors, from CM to the

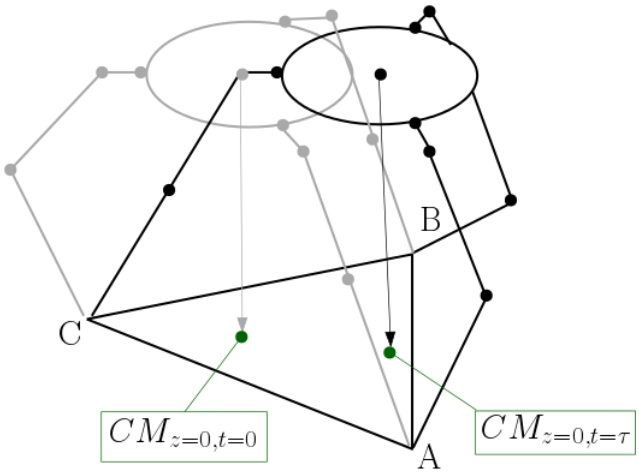

Figure 3.11: The projection of center of mass in to different positions at two different times

hip joint location.

$$r_{a,z}, r_{b,z}, r_{b,z}, r_{c,y} = 0 \tag{3.47}$$

$$r_{a,x} = r_{b,x} \tag{3.48}$$

$$r_{a,y} = -r_{b,y} \tag{3.49}$$

$$\mathbf{F_{tot}} = \begin{bmatrix} f \\ 0 \\ 0 \end{bmatrix} \tag{3.50}$$

$$\mathbf{T_{tot}} = \mathbf{0} \tag{3.51}$$

To prevent rotation of the platform,[11] the properties in equation 3.2 must hold. Note that this is a limiting property in terms of possible $\theta_{1a}, \theta_{1b}, \theta_{1c}$, as the insect-legs lacks spherical hip-joints. This property makes the model similar to the semi-quad in [12], since $O_{1a}||O_{1b}$.

[11] This simplifies the calculations.

$$\mathbf{r_a} \times \mathbf{f_a} + \mathbf{r_b} \times \mathbf{f_b} + \mathbf{r_c} \times \mathbf{f_c} = \mathbf{0} \tag{3.52}$$

$$\begin{bmatrix} r_{a,y}f_{a,z} - r_{a,z}f_{a,y} \\ -r_{a,x}f_{a,z} + r_{a,z}f_{a,x} \\ r_{a,x}f_{a,y} - r_{a,y}f_{a,x} \end{bmatrix} + \begin{bmatrix} r_{b,y}f_{b,z} - r_{b,z}f_{b,y} \\ -r_{b,x}f_{b,z} + r_{b,z}f_{b,x} \\ r_{b,x}f_{b,y} - r_{b,y}f_{b,x} \end{bmatrix} + \begin{bmatrix} r_{c,y}f_{c,z} - r_{c,z}f_{c,y} \\ -r_{c,x}f_{c,z} + r_{c,z}f_{c,x} \\ r_{c,x}f_{c,y} - r_{c,y}f_{c,x} \end{bmatrix} = \begin{bmatrix} 0 \\ 0 \\ 0 \end{bmatrix} \tag{3.53}$$

$$r_{ab,y}(f_{a,z} - f_{b,z}) = 0 \tag{3.54}$$

$$r_{ab,x}(f_{a,z} + f_{b,z}) = -r_{c,x}f_{c,z} \tag{3.55}$$

$$r_{ab,x}(f_{a,y} + f_{b,y}) - r_{ab,y}(f_{a,x} - f_{b,x}) + r_{c,x}f_{c,y} = 0 \tag{3.56}$$

From equations 3.54 to 3.55, one can derive the following,

$$f_{a,z} = f_{b,z} = f_{ab,z}, \tag{3.57}$$

$$f_{c,z} = -2\frac{r_{ab,x}}{r_{c,x}}f_{ab,z}. \tag{3.58}$$

Avoiding movement in y-direction as in equation 3.50, leads to,

$$\mathbf{f_a} = \begin{bmatrix} f_{a,x} \\ f_{a,y} \\ f_{a,z} \end{bmatrix} = \begin{bmatrix} f_{b,x} \\ -f_{b,y} \\ f_{b,z} \end{bmatrix} = \mathbf{f_b} \tag{3.59}$$

$$, \mathbf{f_c} = \begin{bmatrix} f_{c,x} \\ 0 \\ -2\frac{r_{ab,x}}{r_{c,x}}f_{ab,z} \end{bmatrix}. \tag{3.60}$$

Avoiding movement in z-direction as well leads to the relation including the gravity vector,

$$\sum f_z = 2f_{ab,z} - 2\frac{r_{ab,x}}{r_{c,x}}f_{ab,z} - mg = 0, \tag{3.61}$$

$$f_{ab,z} = \frac{mg}{2\left(1 - \frac{r_{ab,x}}{r_{c,x}}\right)}. \tag{3.62}$$

From the solution of $\ddot{x} = f(x, \dot{x})$, a simplistic proposal of desirable force on the platform can be investigated. For a constant $k_1.k_2 \in \mathbb{R}^+$, 3.63 start and stop the

motion in a direction.

$$f_1(t) = \begin{cases} k_1 & 0 \leq t < t_1 \\ 0 & t_1 \leq t < t_2 \\ -k_2 & t_2 \leq t < t_3 \end{cases} \tag{3.63}$$

If d is the distance from the CM at time $t_0 = 0$ to the side, the time intervals can be calculated as in 3.72. This is derived as follows, [15][2]

$$d(t) = d(t_0) + \dot{d}(t_0)t + \frac{1}{2}\ddot{d}(t_0)t^2, \tag{3.64}$$

$$t_0 = t \quad | \quad t = 0, \tag{3.65}$$

$$d_0 = d(t_0), \tag{3.66}$$

$$\dot{d}(t_0) = 0, \tag{3.67}$$

$$d(t_1) = d_0 + \frac{1}{2m}k_1 t_1^2, \tag{3.68}$$

$$\dot{d}(t_1) = \frac{k_1}{m}t_1, \tag{3.69}$$

$$d(t_2) = d(t_1) + \frac{k_1}{m}t_1 t_2, \tag{3.70}$$

$$\dot{d}(t_2) = \frac{k_1}{m}t_1, \tag{3.71}$$

$$d(t_3) = d(t_2) + \frac{k_1}{m}t_1 t_3 - \frac{1}{2m}k_2 t_3^2, \tag{3.72}$$

$$\dot{d}(t_3) = \frac{k_1}{m}t_1 - \frac{k_2}{m}t_3. \tag{3.73}$$

A movement of CM from $d(t_0)$ to $d(t_3)$ displaces the center of mass such that the normal forces on the three legs become as below,

$$n_{ab,z} = \frac{mg}{2}\Big(\frac{d(t)}{h_c}\Big) \tag{3.74}$$

$$n_{c,z} = mg\Big(1 - \frac{d(t)}{h_c}\Big) \tag{3.75}$$

These equations are valid for $CoP \in CP$. Note that this changes if the CP is not an equilateral triangle. Putting the solution, derived in equation3.72, in these equations gives equations,

$$n_{ab,z} = \frac{mg}{2h_c}\big(d_0 + \frac{1}{2m}k_1t_1^2 + \frac{k_1}{m}t_1t_2 + \frac{k_1}{m}t_1t_3 - \frac{1}{2m}k_2t_3^2\big), \tag{3.76}$$

$$n_{c,z} = \frac{mg}{2}\big(1 - \frac{1}{h_c}(d_0 + \frac{1}{2m}k_1t_1^2 + \frac{k_1}{m}t_1t_2 + \frac{k_1}{m}t_1t_3 - \frac{1}{2m}k_2t_3^2)\big). \tag{3.77}$$

Adding the total forces together and calculating the torques leads to the force in 3.63 that can be calculated, given d_0, a initial conditions for the joint variables and a CP. The torques become,

$$\mathbf{f_{0}}_i = \mathbf{n}_i + \mathbf{f_p}_i, \tag{3.78}$$

$$\Longrightarrow$$

$$\mathbf{f_{0}}_{ab} = \mathbf{n_{ab}} + \frac{1}{3}\mathbf{f_p}, \tag{3.79}$$

$$\mathbf{f_{0}}_c = \mathbf{n_c} + \frac{1}{3}\mathbf{f_p}, \tag{3.80}$$

$${\tau_\mathbf{a}}^T(t) = \big[\mathbf{n_{ab}} + \frac{1}{3}\mathbf{f_p}\big]^T\mathbf{J_a}(\mathbf{\Theta_a}), \tag{3.81}$$

$${\tau_\mathbf{b}}^T(t) = \big[\mathbf{n_{ab}} + \frac{1}{3}\mathbf{f_p}\big]^T\mathbf{J_b}(\mathbf{\Theta_b}), \tag{3.82}$$

$${\tau_\mathbf{c}}^T(t) = \big[\mathbf{n_c} + \frac{1}{3}\mathbf{f_p^p}\big]^T\mathbf{J_c}(\mathbf{\Theta_c}). \tag{3.83}$$

The equations 3.81 to 3.83 are vector differential equations where J_a, J_b and J_c are the Jacobians from equation 3.6. These equations lead to the torques for each leg in equations 3.85 to 3.87. Here, f_y and f_z are zero, as earlier. Note that the force f_p^p is expressed in the platform frame.

$${\tau_\mathbf{a}}^T(t) = \big[\mathbf{n_{ab}} + \mathbf{R}_{\phi,\frac{2\pi}{3}}\frac{1}{3}\mathbf{f_p^p}\big]^T\mathbf{J_a}(\mathbf{\Theta_a}) \tag{3.84}$$

Equation 3.84 describes the torques in the same frame as the respective Jacobians. With the x-component of f_p, f_x, the final vectors are described,

$$\tau_{\mathbf{a}}(t) = \begin{bmatrix} \tau_{a,1} \\ \tau_{a,2} \\ \tau_{a,3} \end{bmatrix}$$
$$= \begin{bmatrix} -\frac{1}{2}((\frac{f_x}{3}s(\theta_1)(d_1+d_3c(\theta_2+\theta_3)+d_2c(\theta_2))-(\sqrt{3}f_xc(\theta_1)(d_1+d_3c(\theta_2+\theta_3)+d_2c(\theta_2)))) \\ \frac{1}{2}(\sqrt{3}f_xs(\theta_1)(d_3s(\theta_2+\theta_3)+d_2s(\theta_2))-(f_xc(\theta_1)(d_3s(\theta_2+\theta_3)+d_2s(\theta_2))-(gmd(t)(d_3c(\theta_2+\theta_3)+d_2c(\theta_2))))\frac{1}{h_a} \\ (\frac{1}{2}f_xd_3s(\theta_2+\theta_3)(\sqrt{3}s(\theta_1)-c(\theta_1))-d_3gmc(\theta_2+\theta_3)d(t)\frac{1}{2h_a} \end{bmatrix} \tag{3.85}$$

$$,\tau_{\mathbf{b}}(t) = \begin{bmatrix} \tau_{b,1} \\ \tau_{b,2} \\ \tau_{b,3} \end{bmatrix}$$
$$= \begin{bmatrix} (\frac{\sqrt{3}}{2}f_xc(\theta_1)(d-1+d_3c(\theta_2+\theta_3)+d_2c(\theta_2))-(f_xs(\theta_1)(d_1+d_3c(\theta_2+\theta_3)+d_2c(\theta_2)))) \\ \frac{1}{2}(\sqrt{3}f_xc(\theta_1)(d_3s(\theta_2+\theta_3)+d_2s(\theta_2))-(\sqrt{3}f_xs(\theta_1)(d_3s(\theta_2+\theta_3)+d_2s(\theta_2))-(gmd(t)(d_3c(\theta_2+\theta_3)+d_2c(\theta_2))))\frac{1}{h_b} \\ (\frac{1}{2}f_xd_3s(\theta_2+\theta_3)(c(\theta_1)-\sqrt{3}s(\theta_1))-d_3gmc(\theta_2+\theta_3)d(t)\frac{1}{2h_b} \end{bmatrix} \tag{3.86}$$

$$,\tau_{\mathbf{c}}(t) = \begin{bmatrix} \tau_{c,1} \\ \tau_{c,2} \\ \tau_{c,3} \end{bmatrix}$$
$$= \begin{bmatrix} f_xs(\theta_1)(d_1 + d_3c(\theta_2+\theta_3) + d_2c(\theta_2)) \\ f_xc(\theta_1)(d_3s(\theta_2+\theta_3) + d_2s(\theta_2)) + gm(\frac{d(t)}{h_c} - 1)(d_3c(\theta_2+\theta_3) + d_2c(\theta_2)) \\ d_3f_xs(\theta_2+\theta_3)c(\theta_1) + d_3gmc(\theta_2+\theta_3)(\frac{d(t)}{h_c} - 1) \end{bmatrix}. \tag{3.87}$$

3.2.4 Two-leg stance for tripod model with leg masses << platform mass

The assumption of leg masses equal to zero leads to the fact that the motion of the legs while not supporting the platform is unlimited in different ways. The potential and kinetic energy becomes zero, and movement of legs does not require forces. Hence, another approach must be considered.

As the platform mass is considerably larger than the leg masses, the platform is

assumed to be fixated. Then, the leg movement can be calculated using regular methods like Euler-Lagrange. For the one-leg system, viewed in figure 3.6, the D-H table 3.1 is used. The implementation therefore becomes similar to the one from [29].

The three joints of the insect-like leg is actuated. The motion planning problem therefore becomes a inverse kinematic problem, and can be expressed similarly to motion in section 3.2.2 as long as the foot is not in contact with the surface, or is not affected by any normal force or external forces except gravity. The torques are described by a function of the joint variables only,

$$f_i(\boldsymbol{\Theta}, \dot{\boldsymbol{\Theta}}, \ddot{\boldsymbol{\Theta}}) = \tau_i. \tag{3.88}$$

The desirable trajectory can be expressed as a continuous function of $\theta_1(t)$, $\theta_2(t)$ and $\theta_3(t)$.

$$C_1\big(\theta_1(t), \theta_2(t), \theta_3(t)\big), \tag{3.89}$$

where$C_1^0 : [x_0, y_0, z_0] \rightarrow [x_1, y_1, z_1] \in O_0$ such that,

$$z > 0 \forall t \in (t_0, t_1), \tag{3.90}$$

$$z_0, z_1 = 0, \tag{3.91}$$

$$C_1^0 = \begin{bmatrix} 0 \\ 0 \\ \Delta z \end{bmatrix}, \tag{3.92}$$

when $t = t_0$ or $t = t_1$.

As described in the beginning of section 3.1.3, the inverted pendulum dynamics for the platform is relevant. Assume the CoP is located on the interior of the configuration polygon, $CoP \in CP/\partial CP$. Movement of the free leg is possible during tilting. A sufficiently large force acting on the platform perpendicular to the line between CM of the platform and the support feet, will lead to tilting, but if the angular velocity, $\dot{\phi}_1$, at the unstable equilibrium $\phi_1 = 0$ is negative, the

robot will fall, due to under-actuation. Hence, the strategy of moving CoP to the boundary of the CP during three-leg stance, is not desirable for this specific case. The tilting motion must be limited such that the $\phi_0 > 0 \quad \forall t$, except for a special case[12]. A kicking-from-motion must be introduced, or a motion accelerating the CM. Given an initial angle $\phi_1(0) = \phi_0 > 0$ and assume a three-leg stance where the knee joint $\theta_2 > 0$. Then, a force $\mathbf{f}(\tau_\mathbf{f})$ orthogonal to the line between O_0 and O_p will generate a motion as in equation 3.18. From the equations of motion described in equations 3.17 and 3.18, and the joint torques and mass distribution described in equation 3.9, one can derive a relation describing the swinging motion.
Fixating the length, d, will lead to the standard pendulum equation 3.94. The relation 3.93 describes the property needed for the force to act tangentially on the swinging arm.

$$\mathbf{f}(\tau_f) \cdot \mathbf{P}_a(\theta) = 0 \tag{3.93}$$

$$\ddot{\phi}_1 - \frac{g}{d} \sin \phi_1 = \frac{f_p(\tau_f)}{md} \tag{3.94}$$

This nonlinear ODE is analytically solvable, but the common simplification $sin(\phi_1) \approx \phi_1$ for small ϕ_1 is good enough to give an indication of what the solution of time is like. Using this approximation, leads to equation 3.95 for the initial conditions $\phi_1(0) = \phi_0$ and $\dot{\phi_1}(0) = 0$,

$$\phi_1(t) = \frac{(e^{\sqrt{\frac{g}{d}}t} + e^{-\sqrt{\frac{g}{d}}t})\phi_0}{2} + \frac{\sqrt{d}(I_1 - I_2)}{2md\sqrt{d}}, \tag{3.95}$$

where,

$$I_1 = \Big(\int_0^t e^{-\sqrt{\frac{g}{d}}t} f_p(\tau)\, d\tau \Big) e^{\sqrt{\frac{g}{d}}t},$$
$$I_2 = \Big(\int_0^t e^{\sqrt{\frac{g}{d}}t} f_p(\tau)\, d\tau \Big) e^{-\sqrt{\frac{g}{d}}t}.$$

[12] D in figure 3.10

For $\dot{\phi}_1(0) = \dot{\phi}_0$ and $f_p(t) = 0$ and,

$$\phi_1(t) = \frac{1}{2\sqrt{g}}\big((\sqrt{g}\phi_0 + \sqrt{d}\dot{\phi}_0)e^{\sqrt{\frac{g}{d}}t} + (\sqrt{g}\phi_0 - \sqrt{d}\dot{\phi}_0)e^{-\sqrt{\frac{g}{d}}t}\big). \tag{3.96}$$

The torques for the kicking leg becomes similar to the vector 3.87, with $f_p(\tau_f) = [f_x, 0, f_z]^T$, shown in equation 3.99. For the displacement of center of mass, $l(t)$ this is now a relation between d and ϕ_1,

$$l(t) = d\cos(\phi_1). \tag{3.97}$$

The distance d can be expressed by the position in equation 3.1.2 as the Euclidean distance of the x and z components of the vector,

$$d = \left|\begin{bmatrix} 1 & 0 & 0 \\ 0 & 0 & 0 \\ 0 & 0 & 1 \end{bmatrix}\mathbf{P^p}\right|_2, \tag{3.98}$$

and the torque, as a function of time ande the joint variables, become,

$$\tau_c = \begin{bmatrix} f_x\sin(\theta_1)(d_1 + d_3\cos(\theta_2+\theta_3) + d_2\cos(\theta_2)) \\ (f_z + gm(\frac{l(t)}{h_c} - 1)(d_3\cos(\theta_2+\theta_3) + d_2\cos(\theta_2)) + f_x\cos(\theta_1)(d_3\sin(\theta_2+\theta_3) + d_2\sin(\theta_2)) \\ d_3\cos(\theta_2+\theta_3)(f_z + gm(\frac{l(t)}{h_c} - 1) + d_3 f_x\sin(\theta_2+\theta_3)\cos(\theta_1) \end{bmatrix}. \tag{3.99}$$

In order for the expression of forces 3.99 to be associated with the solution of time 3.95, the external force vector $[f_x(t), 0, f_z(t)]^T$ should satisfy the relation in equation 3.93. Hence, they can be expressed as

$$\begin{bmatrix} f_x(t) \\ 0 \\ f_y(t) \end{bmatrix} = \begin{bmatrix} f_p(t)\cos(\phi_1) \\ 0 \\ f_p(t)\sin(\phi_1) \end{bmatrix}. \tag{3.100}$$

The optimal force-torque ratio can be found using an optimization technique, such as a gradient method from [27], which takes into account the maximum torques of the motors.

Another approach is to accelerate the center of mass in the same way as described in section 3.2.3. Fixating the joint positions of the front legs will, for a sufficiently

high velocity, lead to tilting if the momentum is preserved. The dynamics will be similar. Sudden changes in the stance legs torques, changing from a velocity to fixation in a short period of time, can demand high torque motors.

3.2.5 Motion planning for semi-simple model

There is one passive degree of freedom and several moving masses for the semi-simple model, which suggests that the motion generators $\psi_i(\phi)$ can be found such that the system can balance. The desirable motion does include some other restrictions,

1. The curve foot on swing leg of must satisfy the condition described in relation 3.89

2. The motion should be independent of time

however these might be hard to satisfy. First consider the case where all joint variables are fixated except for the swing leg hip-joint θ_2 , the one orthogonal to the platform z axis, and the passive coordinate ϕ. Assume the hip link is orthogonal when projected onto the xy-plane to the rotation axis of the two stance legs. θ_2 influences the passive degree ϕ. The conservation of spin and momentum and Newton's second law on the CM indicates presence of some degree of controllability. Assuming the effect from the moving center of mass is small leads to a fixated l_0. Inspecting the equation where the mentioned coordinates are fixated, one gain a equation on the form,

$$\alpha(\phi_0)\ddot{\phi}_0 + \hat{g}(\phi_0) + a_0(\cos(\phi_0)\cos(\theta_{2c}) - \sin(\phi_0)\sin(\theta_{2c})) = 0, \tag{3.101}$$

where $g(\phi)$ is a trigonometric function of ϕ, and a_i are constants, and

$$\alpha(\phi_0) = \frac{a_1}{a_2} + \frac{\sqrt{a_1}}{a_2} + a_3. \tag{3.102}$$

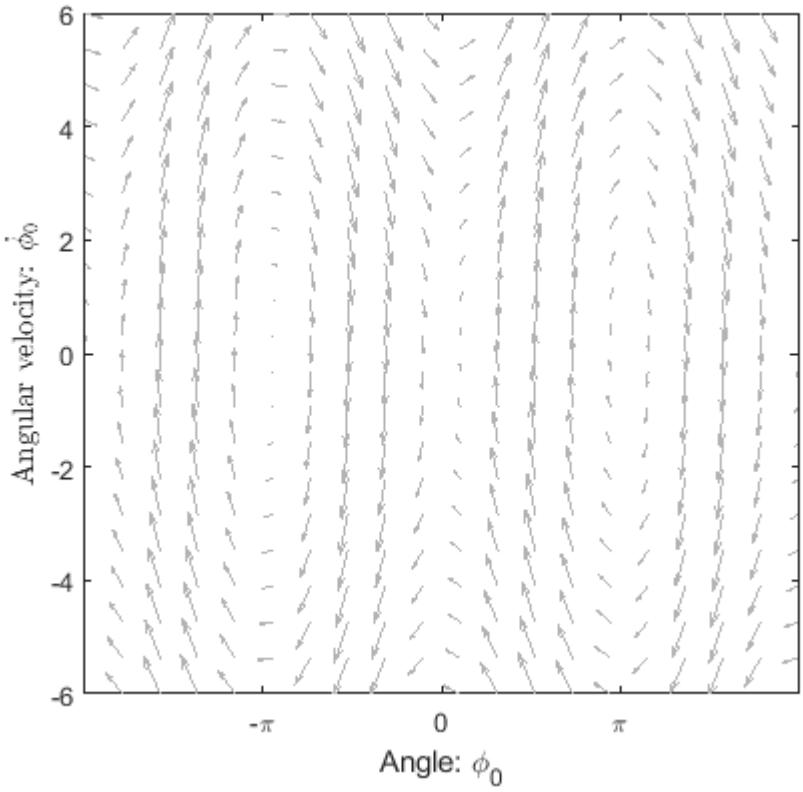

Figure 3.12: Phase portrait of the semi-simple dynamics with fixated values associated with equation 3.101. The point $(\phi_0, \dot{\phi}_0) = (0, 0)$ can be recognized as an unstable equilibrium [14].

The part containing θ_{2c} is,

$$\hat{g}(\phi_0) = (a_4 - a_5 + a_6)\cos(\phi_0) - (a_7 + a_7\sqrt{3} + a_8)\sin(\phi_0). \tag{3.103}$$

For a constant θ_{2c} in equation 3.101 one get the phase portrait depicted in figure 3.12. As expected, this phase portrait can be recognized as the phase portrait of the inverted pendulum, with an unstable equilibrium in $\phi_0 = 0, \quad \dot{\phi}_0 = 0$. The constant $b_1 = 5163$.

A motion generator $\theta_{2c} = \psi(\phi_0)$ can change the phase portrait such that $\phi_0 = 0, \quad \dot{\phi}_0 = 0$ becomes a stable equilibrium, if the integral 2.29 preserves its zero-value for the initial and end values $\phi_0(t=0), \quad \dot{\phi}_0(t=0), \quad \phi_0(t=t_1), \quad \dot{\phi}_0(t=t_1)$. However, solving the integral might not be necessary if the terms it consists of becomes equal to zero. This is shown in the following equations,

$$\begin{aligned}\alpha(\phi_0) = &\frac{b_1}{b_2}M + \frac{b_1}{5b_2}m + \frac{Mr^2}{2} + 2d_1^2 m \\ &+ \frac{d_2^2 m}{2} + \frac{3mr^2}{2} + \frac{\sqrt{b_1}d_1 m}{25} + \frac{d_2 mr}{2} \\ &- \frac{\sqrt{3}Mr^2}{4} + \frac{\sqrt{3}d_2^2 m}{4} - \frac{\sqrt{3}r^2 m}{4}, \end{aligned} \tag{3.104}$$

$$\begin{aligned}\mathbf{g} = &d_2 gm\cos(\phi_0 + \theta_{2c}) - \frac{(\sqrt{b_1}Mg\sin(\phi_0))}{100} \\ &- \frac{(\sqrt{b_1}gm\sin(\phi_0))}{50} - gmr\cos(\phi_0) - 2d_1 gm\sin(\phi_0) \\ &+ \frac{(3\sqrt{2}d_2 gm\cos(\phi_0))}{8} + \frac{(\sqrt{6}d_2 gm\cos(\phi_0))}{8} \\ &- \frac{(\sqrt{2}gmr\cos(\phi_0))}{4} + \frac{\sqrt{6}gmr\cos(\phi_0))}{4} \\ &- \frac{(\sqrt{3}d_2 gm\sin(\phi_0))}{2}, \end{aligned} \tag{3.105}$$

$$\theta_{2c} = f(\phi_0). \tag{3.106}$$

Using the formula for integral of motion 2.29, leads to the integral shown in 3.107. To avoid confusion ϕ_0 become x, such that $x_0 = \phi_0(t=0)$.

$$I(x, \dot{x}, x_0, \dot{x}_0) = \dot{x}^2 - \left[\dot{x}_0^2 - \frac{2}{\alpha}\int_{x_0}^{x} \mathbf{g}(\mathbf{s})ds\right] \tag{3.107}$$

This integral should preserve its zero-value along the solution. Inspecting the formula 3.105, it can be solved for $\theta_{2c}(\phi_0)$. This function is shown in Appendix equations B.2. According to the solver in *MapleSoft* the motion generator is only valid in the interval $[\phi \leq 0.1886019406, -0.04520849592 \leq \phi]$.

The saddle point around $\phi_0 = 0.01, \quad \dot{\phi}_0 = 0$ is possibly skewed due to the assumption considering the center of mass to be equal to the center of the platform. This result suggests inclusion of the displacement of the center of mass due to movement of θ_{2c}. Other factors which becomes clear when inspecting the phase plane is the

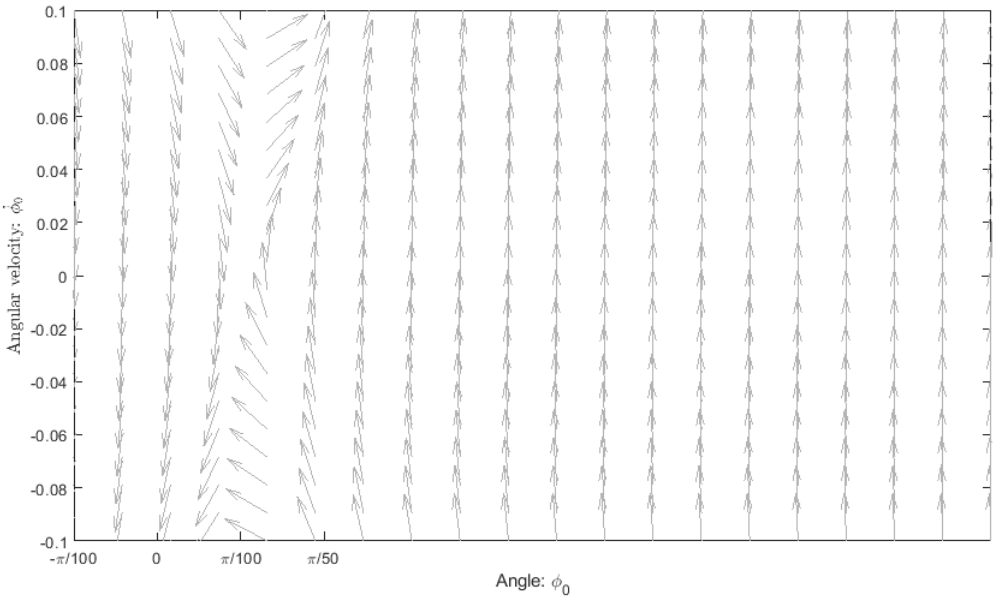

Figure 3.13: Phase portrait of the semi-simple dynamics with fixated values as in 3.12, with the motion generator in equation 3.106.

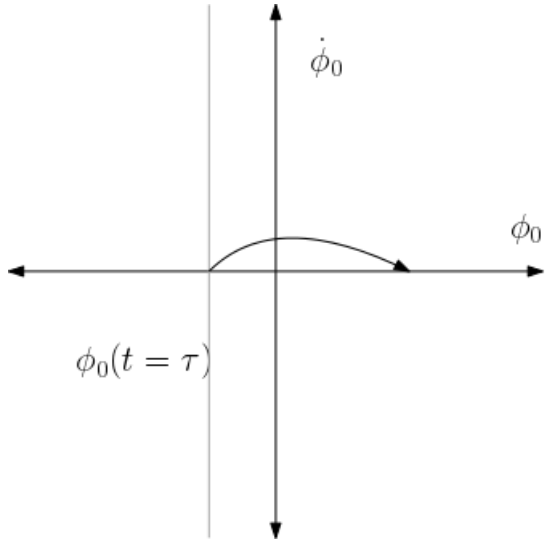

Figure 3.14: The desired motion for the motion when starting two-legged stance with initial position of the CoP outside the CP

fact that the desired actuation necessary to return CoP back to the initial CP is only possible if the angular velocity is already positive, which is a contradiction. This is relevant for the approach where three-leg stance is active until CoP is outside the CP, for lifting of the swing leg.

Another motion generator should be developed. The motion generator derived in 3.106 derived from the integral of motion, was based on finding the function which makes the integrand equal to zero, not dependent on the initial and end positions. Not trying to balance, but rather moving the leg from one position to another in a way that satisfies the conditions 3.89, can be done in the same way as described for finding 3.106.

Finding the motion generator which leads to the motion depicted in figure 3.14, requires investigation of the integral of motion with equation,

$$I(x, \dot{x}, x_0, \dot{x}_0) = \dot{x}^2 - \Big[\frac{2}{\alpha}\int_{x_0}^{x} \mathbf{g}(\mathbf{s})ds\Big], \tag{3.108}$$

This can for $\tau = 0$ be written as

$$I = \dot{x}^2 - \Big[\frac{2}{\alpha}\Big(\int_{x_0}^{x} d_2 gm\cos(s + f(s))\,ds\; + I_1\Big)\Big], \tag{3.109}$$

where I_1 can be found in Appendix B.10

The goal is to find the motion generator satisfying,

$$\theta_{2c}(\phi_0(t = \tau_1)) = k_1 \in \mathbb{R}^-, \tag{3.110}$$

$$\theta_{2c}(\phi_0(t = \tau_2)) = k_2 \in \mathbb{R}^+. \tag{3.111}$$

A possible solution is,

$$\theta_{2c}(\phi_0) = k_1(\phi_0 - \phi_{\tau 2}) + k_1(\phi_0 - \phi_{\tau 1}) + k_3(\phi_0 - \phi_{\tau 2})(\phi_0 - \phi_{\tau 1}). \tag{3.112}$$

Here, the constants $k_1\,, k_2$ are initial and end values of the joint angle θ_{2c}, and k_3 is an adjustable constant. The values $\phi_{\tau i}$ are the angles of ϕ_0 where θ_{2c} should have specific angles. The design of 3.112 is based on Lagrange's method of polynomial interpolation. The goal is to find a k_3 which makes the integral preserve its zero-value,

$$\int_{x_0}^{x} \cos(\phi_0 + \theta_{2c}(\phi_0))\,d\phi_0. \tag{3.113}$$

The integral, shown in B.10, does not lead to any simple formulation for k_3. Fixating the constant values, as well as the end position, gives a indication if this approach leads to a solution. Another problem with this model is the exclusion of a varying l_0. The Motion generator becomes considerably more complicated to derive, as shown in the last part of this section. Assume the support/stance legs have fixated joints,

$$CM_x^p = \frac{m}{3m + M}\big(2(r + \cos(\theta_{2f})(d_1 + d_2\cos(\frac{\pi}{3} - \theta_{1f})) - (r + d_1 + d_2\cos(\theta_{2_s})\big), \tag{3.114}$$

$$CM_z^p = \frac{-m}{3m + M}\big(2d_2\sin(\theta_{2f}) + d_2\sin(\theta_{2_s})\big). \tag{3.115}$$

Using these to calculate l and ϕ, more representative to the actual dynamics of the system leads to,

$$\begin{aligned} l &= l_0 + CM_z^p \\ &= l_0 + \frac{-md_2(2\sin(\theta_{2f}) + \sin(\theta_{2s})}{3m + M}, \end{aligned} \tag{3.116}$$

$$\dot{l} = \frac{\cos(\theta_{2s})\dot{\theta}_{2s}}{3m + M}, \tag{3.117}$$

$$\ddot{l} = \frac{-\sin(\theta_{2s})\dot{\theta}_{2s}^2 + \cos(\theta_{2s})\ddot{\theta}_{2s}}{3m + M}, \tag{3.118}$$

$$\phi = \phi_0 - \arcsin\Big(\frac{-CM_x^p}{l_0}\Big), \tag{3.119}$$

$$\dot{\phi} = \dot{\phi}_0 - \frac{k_2\dot{\theta}_{2s}\sin(\theta_{2s})}{\sqrt{-\big(k_1 - k_2\cos(\theta_{2s})^2 + 1}}, \tag{3.120}$$

$$\begin{aligned} \ddot{\phi} = \ddot{\phi}_0 &- \frac{k_2\ddot{\theta}_{2s}\sin(\theta_{2s})}{\sqrt{-\big(k_1 - k_2\cos(\theta_{2s})^2 + 1\big)}} \\ &- \frac{k_2\dot{\theta}_{2s}^2\cos(\theta_{2s})}{\sqrt{-\big(k_1 - k_2\cos(\theta_{2s})^2 + 1\big)}} \\ &- \frac{k_1^2\dot{\theta}_{2s}^2\sin^2(\theta_{2s})(k_1 - k_2 cos(\theta_{2s})}{\big(-\big(k_1 - k_2\cos(\theta_{2s})^2 + 1\big)\big)^{3/2}}, \end{aligned} \tag{3.121}$$

where the constants are,

$$k_1 = \frac{m}{3m + M}(2(r + \cos(\theta_{2f})(d_1 + d_2\cos(\frac{\pi}{3} - \theta_{1f}))) - r + d_1), \tag{3.122}$$

$$k_2 = d_2. \tag{3.123}$$

It is more useful to substitute l, ϕ into the robot equation 2.28 of ϕ_0,

$$l_0 = l - CM_z^p \tag{3.124}$$

$$\dot{l}_0 = \dot{l} - \frac{\cos(\theta_{2s})\dot{\theta}_{2s}}{3m+M}, \tag{3.125}$$

$$\ddot{l}_0 = \ddot{l} + \frac{\sin(\theta_{2s})\dot{\theta}_{2s}^2 + \cos(\theta_{2s})\ddot{\theta}_{2s}}{3m+M}, \tag{3.126}$$

$$\phi_0 = \phi + \arcsin\left(\frac{-CM_x^p}{l_0}\right) \tag{3.127}$$

$$\dot{\phi}_0 = \dot{\phi} + \frac{k_2\dot{\theta}_{2s}\sin(\theta_{2s})}{\sqrt{-\big(k_1 - k_2\cos(\theta_{2s})^2 + 1}}, \tag{3.128}$$

$$\begin{aligned}\ddot{\phi}_0 = \ddot{\phi} &+ \frac{k_2\ddot{\theta}_{2s}\sin(\theta_{2s})}{\sqrt{-\big(k_1 - k_2\cos(\theta_{2s})^2 + 1\big)}} \\ &+ \frac{k_2\dot{\theta}_{2s}^2\cos(\theta_{2s})}{\sqrt{-\big(k_1 - k_2\cos(\theta_{2s})^2 + 1\big)}} \\ &+ \frac{k_1^2\dot{\theta}_{2s}^2\sin^2(\theta_{2s})(k_1 - k_2 cos(\theta_{2s})}{\big(-\big(k_1 - k_2\cos(\theta_{2s})^2 + 1\big)\big)^{3/2}},\end{aligned} \tag{3.129}$$

These equations are substituted into the scalar robot equation of ϕ_0 and θ. Deriving a motion generator based of the scalar robot equation, now on the form presented in the equation below is not the scope for this thesis,

$$\alpha(\phi, \theta_{2s}(\phi))\ddot{\phi} + \beta(\phi, \theta_{2s}(\phi), \dot{\theta}_{2s}(\phi))\dot{\phi}^2 + g(\phi, \theta_{2s}(\phi), \ddot{\theta}_{2s}(\phi)) = 0 \tag{3.130}$$

3.2.6 Movement of platform during three-leg stance with non-zero leg masses

The model presented in section 3.2.3 is still valid for the more realistic model including leg masses. However, the CM is now a function of the generalized coordinates rather than the center of the platform, similar to the semi-simple model,

$$CM^p(\mathbf{\Theta_a}, \mathbf{\Theta_b}, \mathbf{\Theta_c}) = \frac{1}{M_{tot}}\sum_{i=1}^{10} cm_i^p \cdot m_i, \tag{3.131}$$

Using coordinates for the legs from 3.1 one get the mass distribution in the platform coordinate system, O_0, 3.132. 3.133 shows a more general version where the center of mass of each link is described by a vector l_i. These equations assume the legs are

equal in construction. The matrices A^i refer to the homogeneous transformations associated with the D-H coordinates listed in table 3.1.

$$\begin{aligned} CM^p = \frac{1}{3m_1 + 3m_2 + 3m_3 + m_p}\Big(& m_p + m_1(A_a^0A^1 + A_b^0A^1 + A_c^0A^1)[\frac{d_1}{2}, 0, 0]^T \\ &+ m_2(A_a^0A^1A^2 + A_b^0A^1A^2 + A_c^0A^1A^2)[\frac{d_2}{2}, 0, 0]^T \\ &+ m_3(A_a^0A^1A^2A^3 + A_b^0A^1A^2A^3 + A_c^0A^1A^2A^3)[\frac{d_3}{2}, 0, 0]^T\Big) \end{aligned} \tag{3.132}$$

$$\begin{aligned} CM^p = \frac{1}{3m_1 + 3m_2 + 3m_3 + m_p}\Big(& m_p + m_1(A_a^0A^1 + A_b^0A^1 + A_c^0A^1)\mathbf{l_1} \\ &+ m_2(A_a^0A^1A^2 + A_b^0A^1A^2 + A_c^0A^1A^2)\mathbf{l_2} \\ &+ m_3(A_a^0A^1A^2A^3 + A_b^0A^1A^2A^3 + A_c^0A^1A^2A^3)\mathbf{l_3}\Big) \end{aligned} \tag{3.133}$$

3.3 MATLAB code

This section will briefly describe the main function and modules of the MATLAB code used for the derivation of the symbolic expressions as well as the simulations as well as the work put into the introductory work on 3D simulation. The code used in the thesis can be found at: `https://github.com/paolsen/tripod_master_thesis_code`

3.3.1 Setting up simulation framework

A three dimensional robot with multiple moving parts often becomes impractical analyzing by inspecting two dimensional plots, as both velocities and positions of multiple joint variable become important. The author therefore used an open source solution for simulating and visualizing the dynamic system. *Gazebo* is a free simulation tool designed for robotics applications. Together with ROS, an open source library consisting of useful robotics packages, Gazebo was used to perform three-dimensional simulations. Gazebo uses different file types [13] which describes the geometric and physical parameters of joints and links. The operative

[13] .sdf, .urdf, .xacro, .world, .launch and more.

Name	Functionality
DeriveEL	Takes the Lagrangian and n generalized coordinates and returns n equations of motion
ForwardEulerOrder2D1	Takes analytic acceleration, external force and initial parameters and returns positions, velocities, and accelerations
DH	Takes the four DH-parameters and compute the homogeneous transformation
sym_expression2value	Takes symbolic expression and substitutes vector of symbols with vector of other types
GenRot	Takes Euler-angles and returns the rotation matrix
linVelocity	Takes symbolic positions and the coordinates, and return the velocity matrices, used in linear velocity jacobian
model	This program derives the equations of motion for the full complexity 12-DOF system
leg_move-ment_calculation	Derives the dynamics of a single leg with masses and inertias
torque_calculation	Derives the torques calculated by using the principle of virtual work, and simulates
Two_leg_stance_EL_simple	Derives the motion of the simple inverted pendulum, and simulates
Two_leg_stance_EL_semi_simple	Derives the motion of the semi-simple model, and simulates
InertiaMatrix	Takes mass, velocity jacobians, rotations and inertia dyadics and derives the inertia matrix

Table 3.9: Overview of the different MATLAB functions and scripts used in this thesis.

system used for simulations was Ubuntu Xenial with the ROS Kinetic and Gazebo 7. Other, newer Linux distributions and especially newer versions of Ubuntu was attempted used, with no success. The robot configuration for the specific tripod investigated in this report was implemented in a *.xacro* file, which can be viewed by following the link mentioned earlier, describes the geometry, inertias, masses and joint parameters. The *.xacro* file is a description of the kinematic graph with extensive information. By default, the built in physics simulator in Gazebo simulates based on the .xacro or .urdf [14] file. Gazebo uses *btRigidBody* [7] for simulation.

3.4 The physical tripod

As the building of mechanical and electric components of the physical tripod is described in another report, [30], this section will only focus on the parts directly relevant for this thesis. The early prototype of the physical robot covers a extended set of specifications leading to a design not yet fully optimized for walking. Many of the properties important for a successful physical robot was unknown at the time the project started. These parameters are mainly maximum motor torque needed, optimal length of legs, maximum angular velocity needed for motors all these factors dependent on the masses of the motors and legs. The usual procedure, involving years of mathematical modeling and simulation before actual building, implementation and testing, was not desirable, as the project consists of many different tasks, which needs several versions to reach desired quality. The overall project is in conjunction with a student driven hobby workshop called Omega Verksted, and the people working with the project are not constant and has often a considerable variety in field of study as well as study year.

3.4.1 The leg construction and design

The robotic leg follows similar characteristics in terms of the lengths of the links and the masses, as used elsewhere in this report. As length of the different leg links

[14] .xacro files are a more effective type of .urdf implemented with use of XML syntax

where considered a key parameter in the dynamics of the robot, these were made relatively easy to replace, and produce. Figure 3.15 shows the construction of a almost complete assembled robotic leg. The parts are made of aluminum square pipes, 3-D printed plastic, and various materials used in the electric modules. The use of 3-D printed plastic is the main issue considering the deviation from the optimal leg, as it introduces elasticity. The motors where chosen to be able to lift the legs an angle θ_{max} for a given torque. In case of insufficient available torque, methods using springs such as described in [25], was considered. To detect forces on each leg a series of weight cells are used, here placed from the center of the platform to the hip of each leg. Note that the relation between the weight cells in such a configuration can be nontrivial, considering the fact that the center of mass is not the same at the center of the platform for the more realistic model. Eventually, weight cells should be integrated into the feet, possibly leading to indications of angle between floor and leg [28].

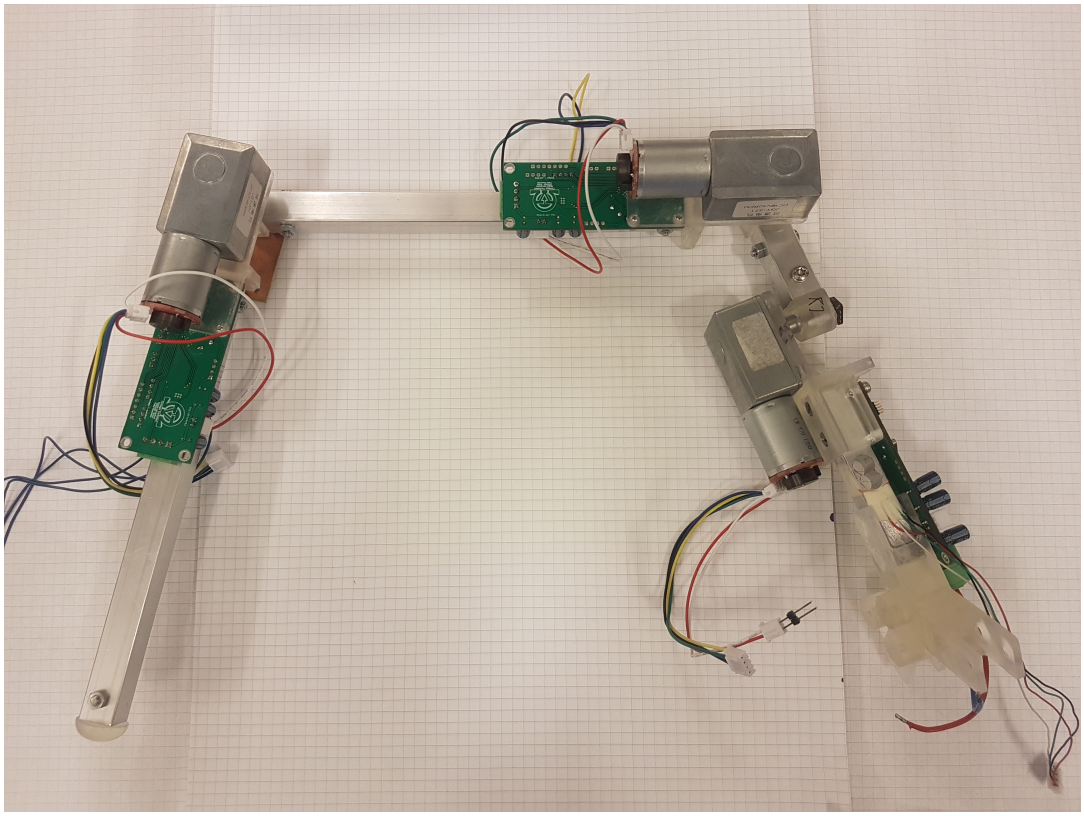

Figure 3.15: Picture of an almost completely assembled robotic leg, attached to the platform bracket.

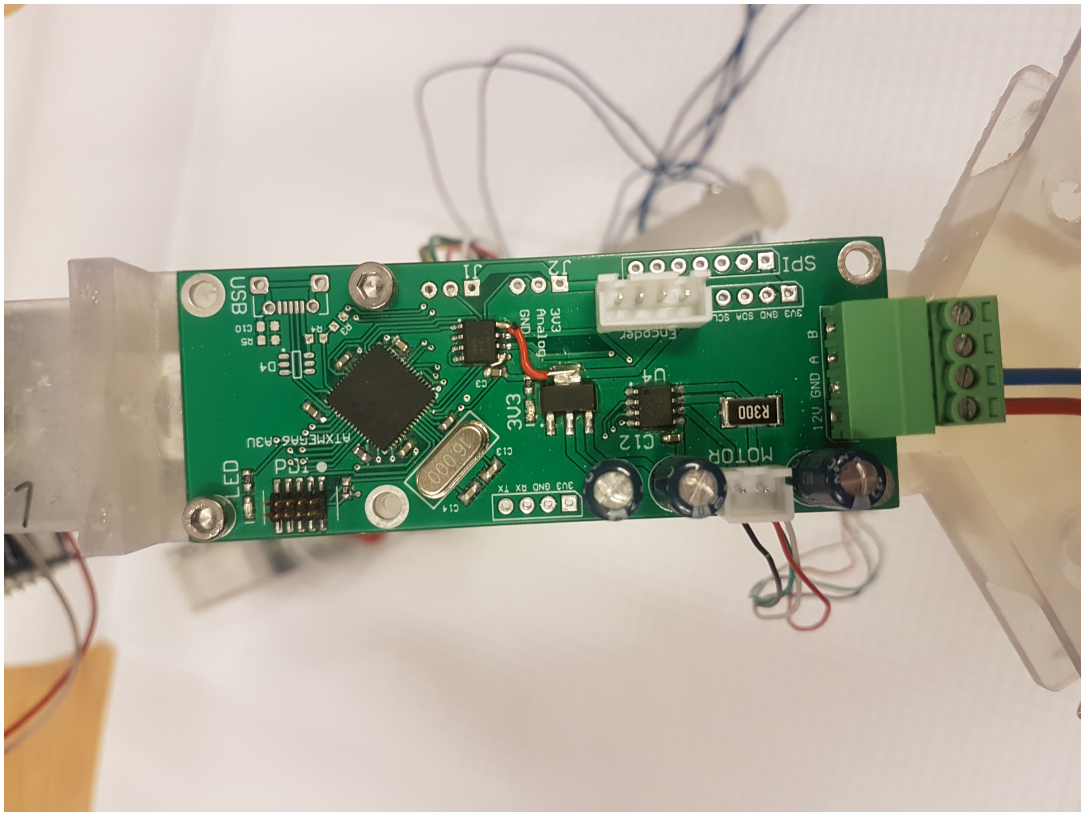

Figure 3.16: Picture of a motor driver designed and produced as part of the overall project.

Voltage $[V]$	Weight1 $[Kg]$	Current1 $[A]$	Weight2 $[Kg]$	Current2 $[A]$	T1 $[Nm]$	T2 $[Nm]$
1,00	1,923	0,089	1,914	0,089	0,0382590	0,0426735
2,00	1,812	0,176	1,785	0,176	0,0927045	0,1059480
3,00	1,650	0,260	1,634	0,261	0,1721655	0,1800135
4,00	1,470	0,340	1,472	0,342	0,2604555	0,2594745
5,00	1,280	0,425	1,250	0,430	0,3536505	0,3683655
6,00	1,090	0,500	1,094	0,503	0,4468455	0,4448835
7,00	1,090	0,531	1,106	0,590	0,4468455	0,4389975
8,00	1,020	0,620	1,018	0,655	0,4811805	0,4821615
9,00	0,998	0,710	0,998	0,702	0,4919715	0,4919715
10,00	0,980	0,770	0,986	0,785	0,5008005	0,4978575
11,00	0,885	0,830	0,845	0,851	0,5473980	0,5670180
12,00	0,628	0,790	0,850	1,200	0,6734565	0,5645655

Table 3.10: A description of measured values for the electric motors used on the early prototype physical tripod. Working torque T_1, stall torque T_2, voltage and current were measured and described in [30].

Chapter 4

Results

In this report some of the results are derived in the methodology section, as analytic equations, some are implemented as programs, and lastly plotted. Some plots of the main models are presented in this chapter.

4.1 Three-leg-stance

the three-leg-stance was analyzed in different variants. As presented in section 3.2.6 the center of pressure can be computed and the simple relation can be used. 4.1 to 4.7 show the torques of the back leg, aligned with the x-axis of the platform, with the parametrization described in 3.46. The joint torque τ_1 is not included as it is constant zero when aligned with the x-axis. By studying the plots and the table 3.10, one can see that the current motors are too weak for such motions with the current parameters.

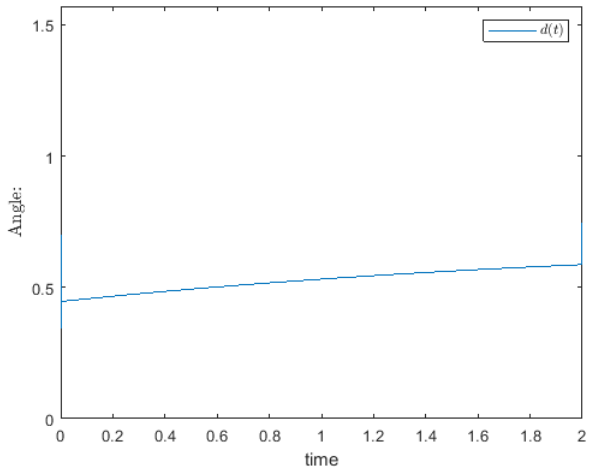

Figure 4.1: Plot of distance between the back foot and the center of pressure for the simplified tripod, based on the parametrization in equation 3.46. The other parameters are: $M = 1$, constant length $d_2, d_3 = 0.4$, $\theta_{2_0} = \pi/6$,$\theta_{3_0} = \pi/3$, height of the configuration polygon $h_c = 0.5$, #Steps = 10000

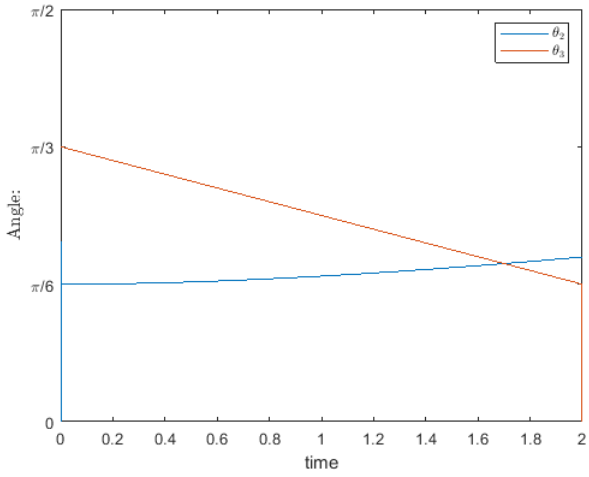

Figure 4.2: Plot of angles associated, and with same parameters as in 4.1

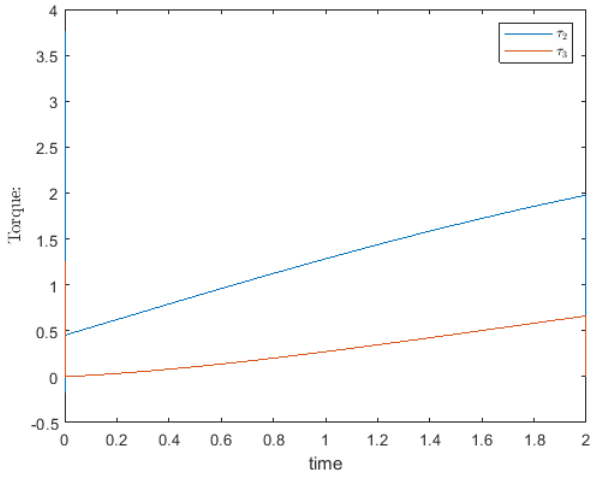

Figure 4.3: Plot of the torques for the back leg associated and with the same parameters as figure 4.1

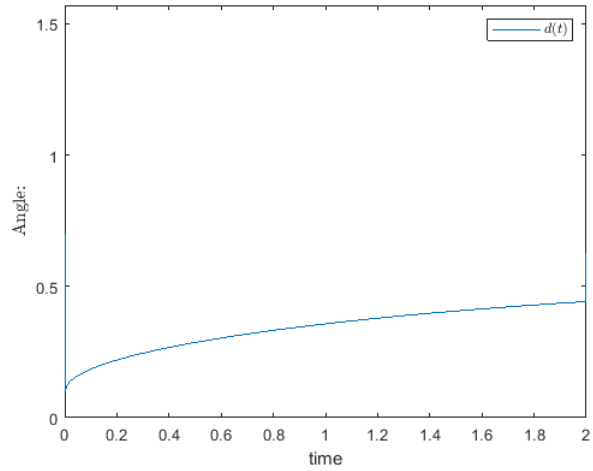

Figure 4.4: Plot of distance between the back foot and the center of pressure for the simplified tripod, based on the parametrization in equation 3.46. The other parameters are: $M = 1$, constant length $d_2, d_3 = 0.4$, $\theta_{2_0} = \pi/3$,$\theta_{3_0} = \pi/3$, height of the configuration polygon $h_c = 1$, #Steps = 10000

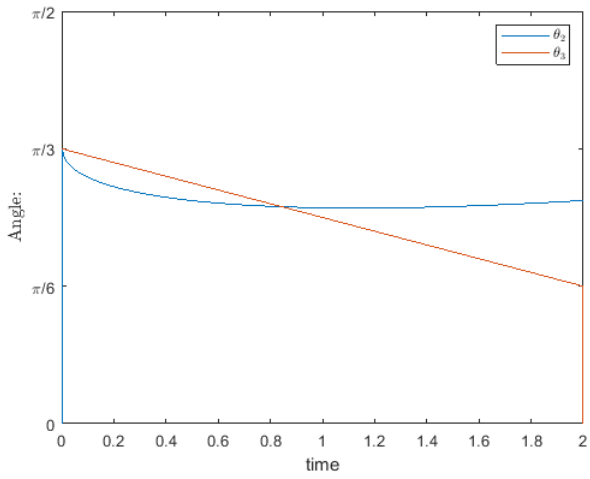

Figure 4.5: Plot of angles associated, and with same parameters as in 4.4

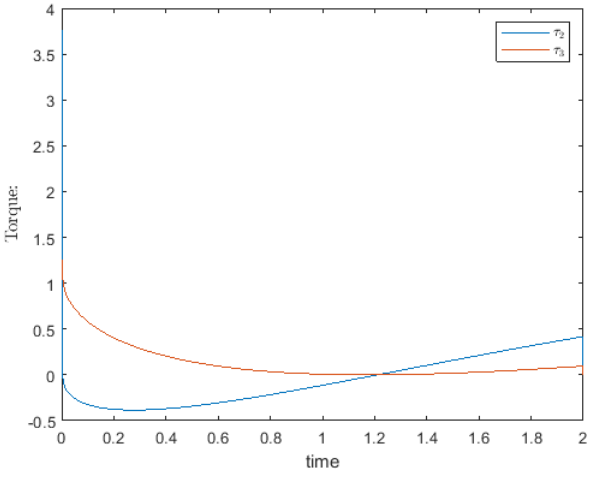

Figure 4.6: Plot of the torques for the back leg associated and with the same parameters as figure 4.4

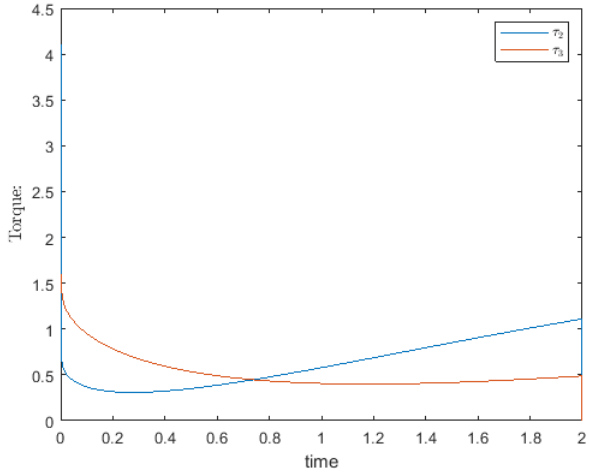

Figure 4.7: Plot of the torques for the back leg associated and with the same parameters as figure 4.4, but with an additional constant force of 1 newton in the negative x axis

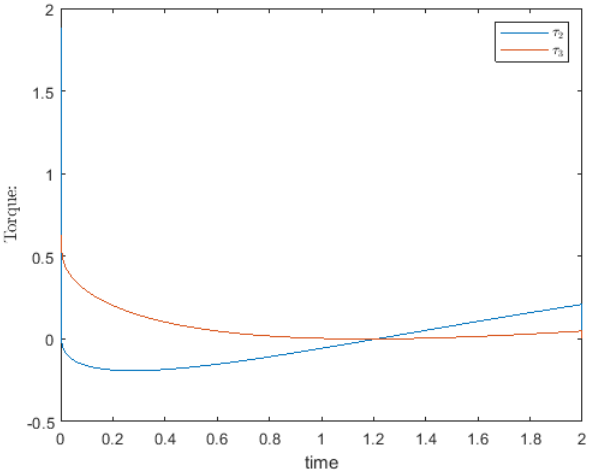

Figure 4.8: Plot of the torques for the back leg associated and with the same parameters as figure 4.4, except for the mass, which is 0.5 kg

4.2 Two-leg-stance

In this section some of the results regarding the two-leg-stance, are presented. Note that the angular values exceeds both the physical limits and 2π in some cases.

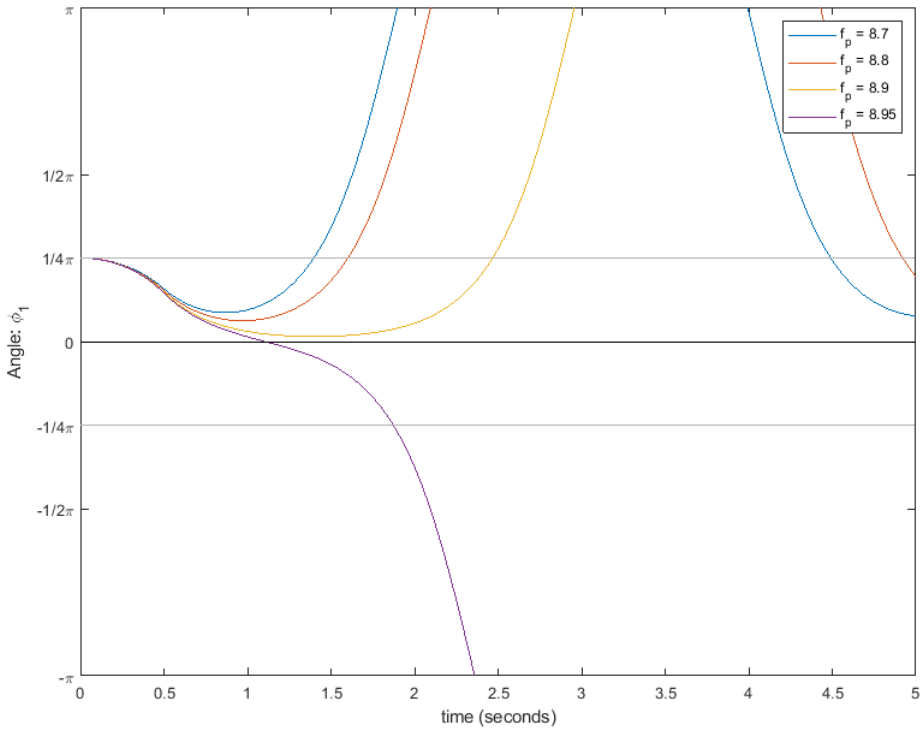

Figure 4.9: Plot of angle ϕ_1 as the perpendicular force for varies in magnitude, with duration of half a second. The other parameters are: $m = 1$, constant length $d = 0.9$ meters which is relevant for the physical tripod. #Steps = 10000

We can calculate the error of the simulations plotted in 4.9 and 4.10, by equation 2.24. It becomes $|\epsilon_5| < 0.4[rad]$, meaning; less than 0.4 radians after 5 seconds, when using 5×10^{-4} as step length, h. Note that the absolute value of the error always should be smaller than the distance to $\phi_1 = 0$, as the equilibrium is unstable.

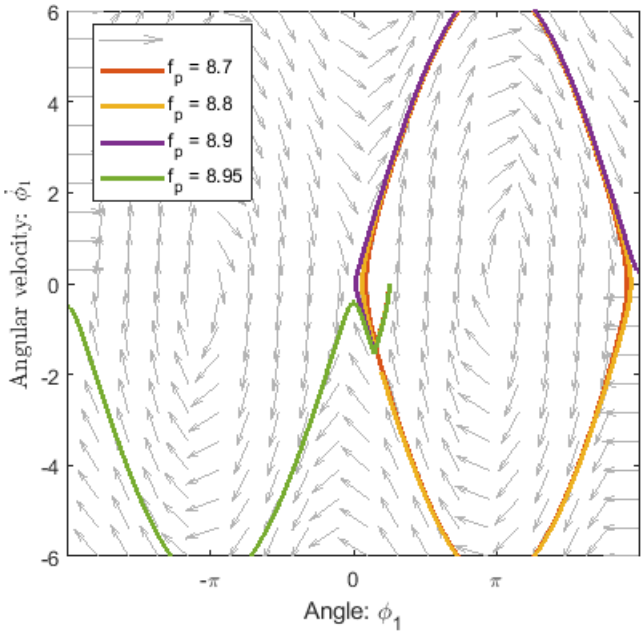

Figure 4.10: Phase portrait of the simple dynamics with normalized arrows. The parameters are the same as in plot 4.9

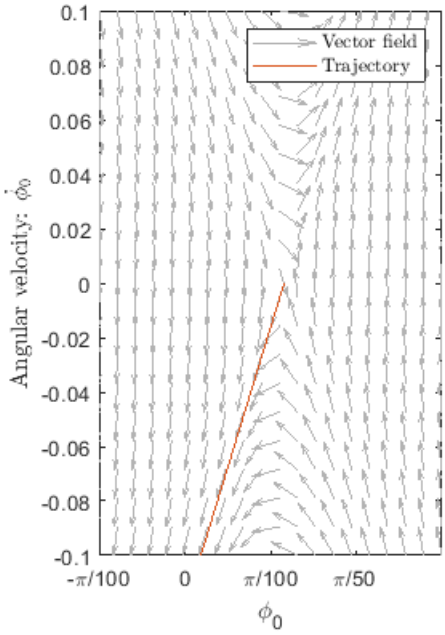

Figure 4.11: Phase portrait of the semi-simple dynamics with normalized arrows. The parameters are the same as in plot 4.9, except for the knee mass $m = 0.5$, with the motion generator shown in Appendix B.2

.

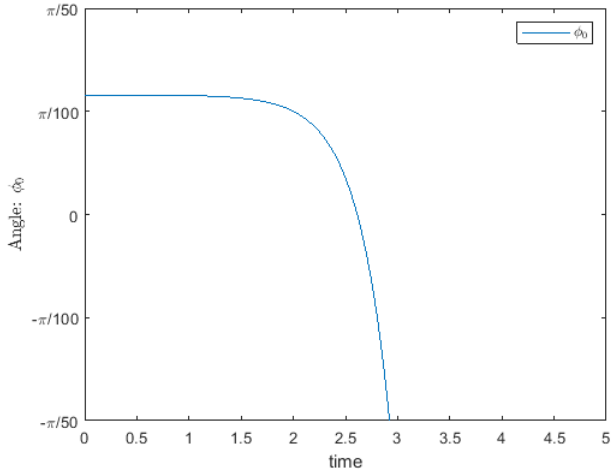

Figure 4.12: Angle of the generalized coordinate associated with the position of center of mass with same parameters as 4.11

.

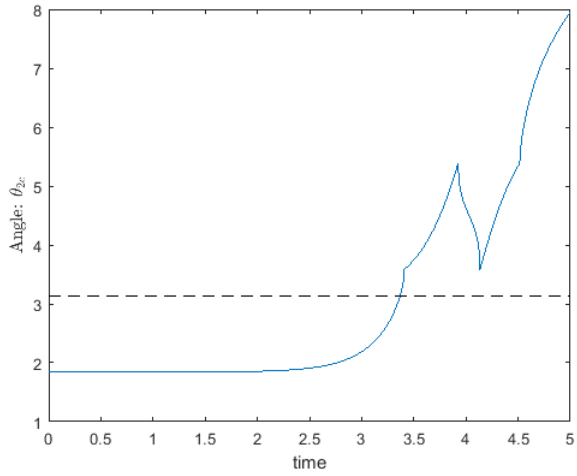

Figure 4.13: Motion of the actuated coordinate with the initial conditions indicated and motion generator shown in equation B.2 in Appendix

.

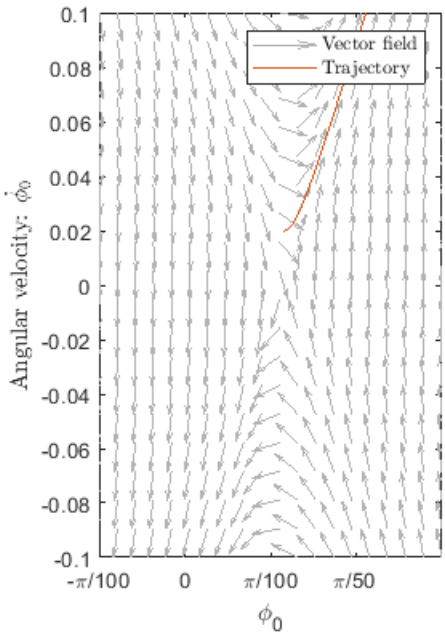

Figure 4.14: Phase portrait of the semi-simple dynamics with normalized arrows. The parameters are the same as in plot, with the motion generator shown in Appendix B.2. Here the initial velocity is positive in $t = 0$

.

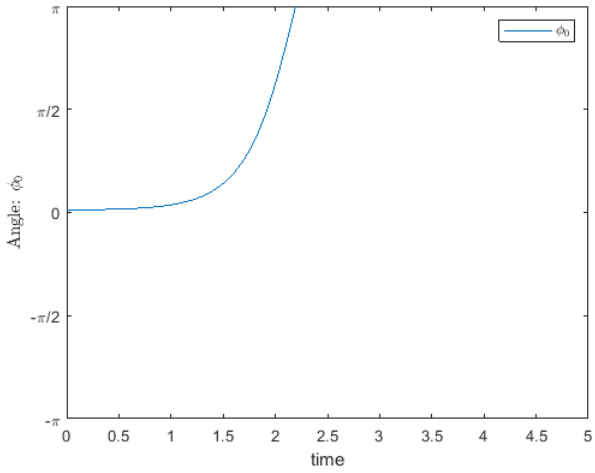

Figure 4.15: Angle of the generalized coordinate associated with the position of center of mass with same parameters as 4.11

.

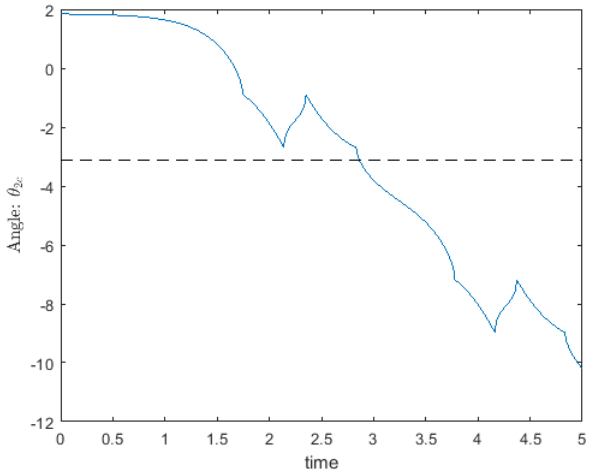

Figure 4.16: Motion of the active coordinate with the initial conditions indicated and motion generator shown in equation B.2 in Appendix

.

4.3 Model in Gazebo

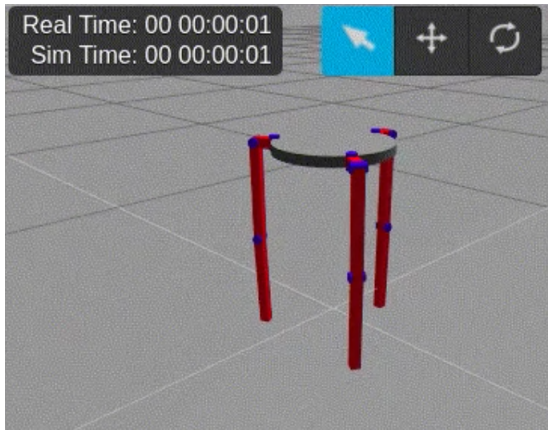

Figure 4.17: Picture from simulation of the passive dynamics simulated by gazebo's internal physics motor. $t = t_0$

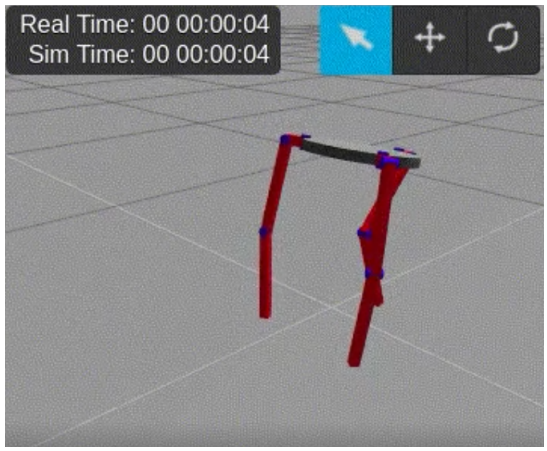

Figure 4.18: Picture from simulation of the passive dynamics simulated by gazebo's internal physics motor. $t = t_1$

Chapter 5

Discussion

5.1 General observations

The method of d'Alemberts principle of virtual work turned out to be a good tool for developing a simple but powerful method on calculating the joint torques and designing associated joint torques needed for specific motions for the three-legged stance. The Euler-Lagrange models using generalized coordinates derived from the Denavit-Hartenberg method were practical describing positions and velocities, but additional coordinates was introduced to better describe the passive dynamics. Parametrization of trajectories and motions for the tripod without adding many constraints such as fixating joint parameters and use symmetric properties to prevent confounding rotations turned out to be time consuming and more complicated than initially believed.

5.2 Development of necessary tools

To be able to analyze the dynamics of the tripod, software able to develop symbolic equations of motion, constraints, and plotting the for given values where crucial. MATLAB was chosen as the main platform from the start, initially because of

the possible integration with Gazebo, and possibility to use *Simulink*, a software package suitable for control theory. Other possibilities where *Python*, and various modeling tools such as *Modelica*. As the prior preparatory investigation in [29] led to different MATLAB programs, these where re-implemented and validated at the beginning of the thesis, and used for most of the calculations, as derivation of dynamic models, equations of motion, simulation and plotting. The main problems with using the symbolic tools in MATLAB where simplification of the models, and time consuming compilation. The latter is partially due to ineffective code. hence, MapleSoft were used to derive some of the analytic expressions for the proposed motion generators. As simulations in 3D can be powerful tools analyzing 3-D robots. However the development working with Gazebo and ROS was time consuming and demanding, regarding how to provide exact packages. The work on the simulations stopped when customized plug-in for Python was needed in order to control the joint parameters. If Python was used as the main programming language from the beginning, the work on the 3-D simulations would have continued. [16] describes how to solve most of the problems touched with MATLAB, in Python. Even if the plug-in was not created and tested for this thesis, the configuration of the robot was developed and the simulation using the inbuilt physics of Gazebo was tested. A necessary feature for further testing is a program generating the initial stance of the robot, as the xacro/urdf/sdf-files are relatively time consuming to create. Newer versions of Gazebo allow trigonometric functions in these files, in contrast to the version used in this study.

The programs for deriving the equations of motion as well as simulating, described in section 3.3, were developed generally, but often includes some formulas derived using MapleSoft. The functions performing standard tasks as deriving the Euler-Lagrange equations, were implemented from scratch, since the alternatives, such as *MATLAB Robotics Toolbox*, did not provide symbolic equations in a preferable way.

5.3 Representation of the coordinates

In terms of describing the positions of the ten links for the tripod, several different approaches where tested. For the complete models as the model analyzed in [29], and the one defined by 3.2, inspection and analysis of the analytic expression is not preferred. The two full complexity representations of the dynamic models lead to the same limitations. Even if the first initially had more equations, with three redundant, and the other, with 12 equations, resulted in different amount of analytical data, significant reductions in parameters [1] did not give valuable information. Numerical analysis would be more relevant for the purpose of simulating the full complexity model, in 3-D.

Simplification by restricting rotational axes and fixating joint variables to a constant value, as well as removing masses and inertias from the full complexity model were performed and lead to the most important results in this thesis. For the purpose of describing motions strongly related to inverse pendulum-movement, introduction of length and angle from swinging axis to center of mass became crucial. For the simplest model these coordinates were trivial. Adding masses to the knees for a more realistic model, these simple coordinates were still tested, under the assumption of small displacement due to small angular difference. However, the generalized coordinate intended to describe the angle from the axis of rotation to the center of mass, required complex modifications. The assumption therefore, did not fit the reality, and as expected, the derived motion generator did not lead to a desired trajectory for the system. The exact representation of the position of center of mass introduced a need for an additional motion generator as the non-constant length of the pendulum introduced extra independent variables in the scalar robot equation.

[1] Parameters with symbolic values were set to a constant numerical value.

5.4 Usefulness of a simplified model

The simplified model considering the platform mass sufficiently larger than the masses of the legs, is often used in previous literature such as [23] and [17]. Even if the assumption is not realistic, the kick-and-swing gait, can be relatively easy to describe with this model. The angular acceleration due to swinging of the free leg can be calculated separately, and a constraint on the kicking force can be introduced for such a gait to be used for a model deviating from the simple model. These gaits are similar to [23], [17] and [12], called the kick-and-swing gait, seems to be a preferable strategy for three-legged locomotive robots. As seen in the plot 4.9, even if a margin is wanted[2], the period of the swing leg, from the start of the lift-of until it lands, is sufficiently long for a realistic robotic leg to manage repositioning, dependent on the position of the new step. A special case depicted as (D) in figure 3.10, allows longer periods, or a shorter pendulum length.

5.5 Three-leg motion

As seen in the plots 4.1 to 4.7, the simple model of the three-leg-stance shows reasonable torque angle ratio. For the tripod the torques while in three-leg-stance is increasing as the angles on the floor gets slacker, more prominent than the effect from a CoP moving away from the corner of the CP. By studying the plots and the table 3.10, one can see that the current motors are too weak for such motions with the current parameters. However as indicated in 4.8, weight-reduction afflicts the needed force, as expected. Hence, limiting the weight of the robot is an important task. For the case of the physical tripod, this can become challenging with current motors.

[2]Keeping a safe distance from the unstable equilibrium.

5.6 Two-leg motion

The two-leg stance introduces a passive DOF, namely the angle between the floor and the center of mass. For the simplified version the tripod becomes equal to an inverted pendulum and the dynamics of the tilting motion can be solved analytically for small angle deviation and numerically for the general case[3]. The force as a function of time can be derived solving an integral equation. For the semi-simple model, adding knee-masses in the model now introducing a angle θ_{2c} influencing both the center of mass, and hence, the generalized passive coordinate and the length of the pendulum. The assumptions considering the displacement of the center of mass leading to the phase portrait 3.12 did not represent the actual position of the CM. Hence, he motion generators developed based on this assumption did not lead to a successful trajectory for the actual system. Relation between the generalized passive coordinate and the actual angle from the ground to the CM, was expressed, and lead to a coordinate transform. However, the updated robot equation substituted with this transform proved to be too complex for this thesis. This suggests further research on the motions for the semi-simple tripod.
In the plots 4.13 and 4.16, the positions of the actuated coordinate is non-smooth which can be hard to achieve in practice, as there might be discontinuous derivatives [15]. The more realistic variant would therefore deviate from the ones presented.

[3]It can also be solved analytically for the general case, but this is not done in this report.

Chapter 6

Conclusion

The tripod with platform mass considerably larger than the leg masses was analyzed for stances where three or two legs were supporting the weight. D'Alembers principle of virtual work was used to describe the torques associated with the joints at each leg for different situations. A model describing how the position of center of pressure affects the expected normal forces, together with other external forces, was found.

For the simplified model, the strategy of moving center of pressure outside of the configuration polygon is not desirable except for a special case [1]. This is due to the unstable equilibrium and lack of controllability when the swing leg is lifted from the ground and the tripod stands on two legs. When the knee masses are non-zero, a similar behaviour was found. The analysis of the different models and their associated movements gave rise to a initial description of different strategies for lifting a leg, and moving the platform in three-leg stance.

[1] case D in figure 3.10

6.1 Future work

For the tripod project there are several tasks still unsolved. The analysis incorporated in this report only scratches the surface of the subject. Even if there are many various, interesting tasks needing investigation, there are some which are crucial, and these are the subject for this section.

- Make a 3D-simulation framework for the tripod working such that models and motions can be tested and verified.
- Development of impact models for impacts described in 2.18. The dynamic models described in this thesis can be used as a basis.
- The situations for one-leg stance should be modeled and analyzed
- Solving the transverse linearization problem
- Developing feedback laws and a controller for the system

Bibliography

[1] Bjoern K. Alsberg. *Chemometrics; version 0.56*. Compendium for TKJ4175/KJ8175. Department of Chemistry; NTNU, 2017. ISBN: 978-82-999127-0-9.

[2] Jens G. Balchen, Trond Andresen, and Bjarne A. Foss. *Reguleringsteknikk*. Institutt for teknisk kybernetikk,NTNU, 2003. ISBN: 82-471-5147-2.

[3] E. R. Booser et al. *Avoiding bearing wear and damage during start-up and shut down*. May 2011. URL: `https://www.machinedesign.com/news/avoiding-bearing-wear-and-damage-during-start-and-shut-down`.

[4] Christine Chevallereau et al. "RABBIT: A Testbed for Advanced Control Theory". In: *IEEE Control Systems Magazine* (Oct. 2003), pp. 57–77.

[5] John J. Craig. *Introduction to Robotics*. Pearson Education, 2006. ISBN: 0-13-123629-6.

[6] Lars Cremean et al. "The Calteck Multi-Vehicle Wireless Testbed". In: *Conference on decision and control (CDC)* (- 2002), pp. 251–253.

[7] Doxygen. *Bullet Collision Detection Physics Library*. Jan. 2019. URL: `https://pybullet.org/Bullet/BulletFull/classbtRigidBody.html`.

[8] Olav Egeland and Tommy Gravdahl. *Modeling and Simulation for Automatic Control*. Marine Cybernetics AS, 2003. ISBN: 82-92356-01-0.

[9] Mats Ernström. *lecture notes in TMA4145 Linenar Methods*. Aug. 2013. URL: `https://www.math.ntnu.no/emner/TMA4145/2013h/lecturenotes27aug.pdf`.

[10] John B. Fraleigh. *Abstract Algebra*. Pearson, 2006. ISBN: 78-81-775-8900-9.

[11] Stephen H. Friedberg, Arnold J. Insel, and Lawrence E. Spence. *Linear Algebra*. Pearson Education, 2003. ISBN: 0-13-120266-9.

[12] Harald Hareide. "Creation and Control of Gaits for the SemiQuad Robot". In: *NTNU Master Thesis* (May 2014), pp. 1–76.

[13] Masato Ishikawa, Naoto Yasutani, and Ryoichi Kuratani. "On Decenteralized Control of Tripedal Walking Robot Using Reaction Force Feedback". In: *Proceedings of CALWAR 2017: 20th International Conference on Climbing and Walking Robots and the Support Technologies for Mobile Machines* (Sept. 2017), pp. 431–438.

[14] Hassan K. Khalil. *Nonlinear Systems*. Pearson Education, 2002. ISBN: 0-13-067389-7.

[15] Erwin Kreyszig. *Advanced Engineering Mathematics*. John Wiley & Sons, 2011. ISBN: 978-0-470-64613-7.

[16] Hans Petter Langtangen. *A primer on Scientific Programming with Python*. Springer, 2002. ISBN: 978-3-642-30292-3.

[17] Yun-Jung Lee and Shigeo Hirose. "Three-Legged Walking for Fault Tolerant Locomotion of a Quadruped Robot with Demining Mission". In: *Proceedings of the 2000 IEEE/RSJ International Conference on Intelligent Robots and Systems* (2000), pp. 973–978.

[18] Jan R. Lien and Gunnar Løvhøyden. *Generell Fysikk*. Universitetsforlaget, 2010. ISBN: 978-82-15-00005-3.

[19] R.Q. van der Linde and A. L. Schwab. "Multibody Dynamics B". In: *Multibody Dynamics B Lecture Notes* (Jan. 1997), pp. 1–30.

[20] Tom Lindstrøm and Klara Hveberg. *Flervariabel Analyse med Lineaer Algebra*. Person Education, 2011. ISBN: 978-0-273-738138.

[21] Anders Malthe-soerenssen. *Introduction to Mechanics; Integrating numerical and analytical methods*. Department of physics; University of Oslo, 2013. ISBN: -.

[22] Sylvan Martel et al. "Three-Legged wireless Miniature Robots for Mass-scale Operations At the Sub-Atomic Scale". In: *Proceedings of the 2001 IEEE International Conference on Robotics & Automation* (May 2001), pp. 3423–3428.

[23] Yoichi Masuda and Masato Ishikawa. "Simplified Triped Robot for Analysis of Three-Dimensional Gait Generation". In: *Journal of Robotics and Mechatronics Vol.29No.3* (Feb. 2017), pp. 528–534.

[24] Uwe Mettin et al. "Motion planning for humanoid robots based on virtual constraints extracted from recorded human movements". In: *Intel Serv Robotics (2008)* (June 2008), pp. 289–301.

[25] Uwe Mettin et al. "Parallel Elastic Actuators as a Control Tool for Preplanned Trajectories of Underactuated Mechanical Systems". In: *International Journal of Robotics research* (Aug. 2009), pp. 1186–1197.

[26] Knut Mørken. *Numerical Algorithms and Digital Representation*. Aug. 2013. URL: `https://www.uio.no/studier/emner/matnat/math/MAT-INF1100/h13/kompendiet/matinf1100.pdf`.

[27] Jorge Nocedal and Stephen J. Wright. *Numerical Optimaization*. Springer Series in Operation Research an Financial Engeneering. Springer, 2006. ISBN: 0-387-30303-0.

[28] Odd Arild Olsen. *Instrumenteringsteknikk*. tapir akademisk forlag, 2006. ISBN: 978-82-519-0926-0.

[29] Per Anton Øverseth Olsen. "Analysis and design of gaits for three-legged walker". In: *NTNU Project Report* (June 2018), pp. 1–51.

[30] Per Anton Øverseth Olsen et al. "Trebeint robot". In: *NTNU Report in subject TFE4205 Spring 2018* (May 2018), pp. 1–106.

[31] Peter Van Overschee and Bart De Moor. *Subspace Identification for Linear Systems*. Springer US, 1996. ISBN: 978-1-4613-0465-4.

[32] Kerry M. Peterson and L. Cagnasso. "Bearing investigation". In: *SKF(2008)* (- 2008), pp. 122–135.

[33] R.C.Hibbeler. *Engineering Mechanics- Dynamics*. Pearson Education, 2007. ISBN: 0-13-203809-9.

[34] Anton Shiriaev, John W. Perram, and Carlos Canudas-de-Wit. "Constructive Tool for Orbital Stabilization of Underactuated Nonlinear Systems: Virtual Constraints Approach". In: *IEEE Transactions On Automatic Control, Vol.50 No 8* (Aug. 2005), pp. 1164–1175.

[35] Anton Shiriaev et al. "Periodic motion planning for virtually constrained Euler-Lagrange systems". In: *Systems & Control Letters 55* (June 2006), pp. 900–907.

[36] Manuel F. Silva and J. A. Tenreiro Machado. "A Historical Perspective of Legged Robots". In: *Journal of Vibration and Control* (May 2006), pp. 1447–1486.

[37] Mark W. Spong, Seth Hutchinson, and M. Vidyasagar. *Robot Modeling and Control*. John Wiley & Sons, Inc, 2006. ISBN: 978-0-471-64990-8.

[38] John T. Wen and John F. O'Brien. "Singularities in Three-Legged Platform-Type Parallel Mechanisms". In: *IEEE Transactions on Robotics and Automation, Vol. 19, No. 4* (Aug. 2003), pp. 720–726.

[39] Guilin Yang et al. "Singularity Analysis of Three-Legged Parallel Robots Based on Passive-Joint Velocities". In: *IEEE transactions on Robotics and Automation VOL 17 No 4* (Aug. 2001), pp. 413–422.

Appendix A

Acronyms

NED North East Directed coordinate system. (x-axis directed north, y-axis directed east, and z-axis directed down)

DOF Degree(s) of freedom

CP Configuration Polygon

CM Center of Mass

CoP Center 0f Pressure

ROS Robot Operating System

URDF Unified Robot Description Format

XML Extensible Markup Language

ODE Ordinary Differential Equation

Appendix B

Equations

B.1 Theorems and lemmas

From [35] we have the *sufficient conditions for existence of periodic solutions of the scalar robot equation, 2.28.* Theorem 3 in [35] states the following:

When q_0 is a equilibrium of 2.28, these sufficient conditions are are:

1. There is a vicinity $\mathcal{O}$ of q_0 such that the scalar functions α, β, and γ are continuous on $\mathcal{O}$, i.e. $\alpha(q), \beta(q), \gamma(q) \in C^0(\mathcal{O})$.

2. There exists a continuous time derivative of $\frac{\gamma(q)}{\alpha(q)}$ at the equilibrium.

3. For any initial conditions $q_0 \in \mathcal{O}$, $\dot{q}_0$ with $|\dot{q}_0| < \delta, \delta > 0$, the corresponding solution of the nonlinear system 2.28 that originates in this point, is well defined and unique.

Consider the system in equation B.1. If this system has a center at $z = 0$, then the nonlinear system 2.28 also has a center at the equilibrium q_0.[1].

$$\frac{d^2}{dt^2}z + \Big[\frac{d}{dq}\frac{\gamma(q)}{\alpha(q)}\Big]|_{q=q_0} \cdot z = 0 \tag{B.1}$$

[1] End of theorem

B.2 calculated values and relations

$$\begin{aligned}\theta = -\phi + \big[&\frac{1}{200\, d_2\, m}(100\,\sqrt{3} d_2\, m \sin(\phi) \\ &- 75\,\sqrt{2} d_2\, m \cos(\phi) \\ &+ 50\,\sqrt{2} m r \cos(\phi) - 25\,\sqrt{6} d_2\, m \cos(\phi) \\ &- 50\,\sqrt{6} m r \cos(\phi) \\ &+ 2\,\sqrt{5163} M \sin(\phi) + 4\,\sqrt{5163} m \sin(\phi) \\ &+ 400\, d_1\, m \sin(\phi) \\ &+ 200\, m r \cos(\phi))\big] \end{aligned} \tag{B.2}$$

This function is valid for the values of ϕ listed in equation

$$[\phi \leq -6.094583367, -6.328393803 \leq \phi], \tag{B.3}$$

$$[\phi \leq -2.952990713, -3.186801150 \leq \phi], \tag{B.4}$$

$$[\phi \leq 0.1886019406, -0.04520849592 \leq \phi], \tag{B.5}$$

$$[\phi \leq 3.330194594, 3.096384158 \leq \phi], \tag{B.6}$$

$$[\phi \leq 6.471787248, 6.237976811 \leq \phi], \tag{B.7}$$

$$[\phi < 9.496474683, 9.379569465 \leq \phi], \tag{B.8}$$

$$\tag{B.9}$$

with $d_2 = 0.4, d_1 = 0.1, m = 0.5, M = 1, r = 0.12$

Motion generator calculation for 2. semi-simple model with start and stop values $\psi_{0\,1}$.

$$
\begin{aligned}
I_1 = & -\frac{\sqrt{b}Mg\cos\left(\psi_0\right)}{100} \\
& - \frac{1}{50}\sqrt{b}mg\cos(\psi_0) \\
& + gmr\sin(\psi_0) - 2\,d_1\,gm\cos(\psi_0) \\
& + 3/8\,\sqrt{2}d_2\,gm\cos(\psi\_0) \\
& + 1/8\,\sqrt{2}\sqrt{3}d_2\,gm\cos(\psi_0) \\
& + 1/4\,\sqrt{2}rgm\sin(\psi_0) - 1/4\,\sqrt{2}\sqrt{3}rgm\sin(\psi_0) \\
& - 1/2\,\sqrt{3}d_2\,gm\cos(\psi_0) \\
& + \frac{\sqrt{b}Mg\cos(\psi_1)}{100} + \frac{1}{50}\sqrt{b}mg\cos(\psi_1) \\
& + 2\,d_1\,gm\cos(\psi_1) - gmr\sin(\psi_1) - 3/8\,\sqrt{2}d_2\,gm\cos(\psi_1) \\
& - 1/4\,\sqrt{2}rgm\sin(\psi_1) + 1/2\,\sqrt{3}d_2\,gm\cos(\psi_1) \\
& - 1/8\,\sqrt{2}\sqrt{3}d_2\,gm\cos(\psi_1) \\
& + 1/4\,\sqrt{2}\sqrt{3}rgm\sin(\psi_1)
\end{aligned}
\tag{B.10}
$$

Per Anton Øverseth Olsen

Analysis of Tripods for Walking Purposes

NTNU
Kunnskap for en bedre verden